11-10-2021

Investigating the Impacts of Sea Level Rise-induced High Groundwater Table on Florida Flexible Pavement Structural Performance

Mehmet Goksel Gocmez
mgocm001@fiu.edu

FLORIDA INTERNATIONAL UNIVERSITY

Miami, Florida

INVESTIGATING THE IMPACTS OF SEA-LEVEL RISE-INDUCED HIGH GROUNDWATER TABLE ON FLORIDA FLEXIBLE PAVEMENT STRUCTURAL PERFORMANCE

A thesis submitted in partial fulfillment of

the requirements for the degree of

MASTER OF SCIENCE

in

CIVIL ENGINEERING

by

Mehmet Goksel Gocmez

2021

To: Dean John L. Volakis
College of Engineering and Computing

This thesis, written by Mehmet Goksel Gocmez, and entitled Investigating the Impacts of Sea-Level Rise-induced High Groundwater Table on Florida Flexible Pavement Structural Performance, having been approved in respect to style and intellectual content, is referred to you for judgment.

We have read this thesis and recommend that it be approved.

_____
Priyanka Alluri

_____
Hector R. Fuentes

_____
Hesham Ali, Major Professor

Date of Defense: November 10, 2021

The thesis of Mehmet Goksel Gocmez is approved.

_____
Dean John L. Volakis
College of Engineering and Computing

_____
Andrés G. Gil

Vice President for Research and Economic Development
and Dean of the University Graduate School

Florida International University, 2021

ABSTRACT OF THE THESIS

INVESTIGATING THE IMPACTS OF SEA-LEVEL RISE-INDUCED HIGH GROUNDWATER TABLE ON FLORIDA FLEXIBLE PAVEMENT STRUCTURAL PERFORMANCE

by

Mehmet Goksel Gocmez

Florida International University, 2021

Miami, Florida

Professor Hesham Ali, Major Professor

This thesis evaluates the impacts of sea-level rise-induced high groundwater table on the structural performance of typical Florida interstate, arterial, and local flexible pavements. Pavement longevity was determined under rising groundwater table level conditions using two analytical methods; the mechanistic-empirical (ME) analysis software and the current Florida empirical analysis practice. Moreover, ABAQUS and KENLAYER software were utilized to analyze the impacts of stress-dependent material nonlinearity on pavement structural performance.

Analysis results estimated that the pavement service life in Florida was reduced by as much as 77 percent with the effects of rising groundwater levels. The empirical method predicted higher rates of pavement deterioration than the ME method. The predominant pavement failure mode was found to be rutting, and higher class roads (interstate and arterial) were found to face more structural capacity loss than local roads. The effects of nonlinear material behavior were found to be insignificant.

TABLE OF CONTENTS

CHAPTER PAGE

LIST OF TABLES

TABLE PAGE

LIST OF FIGURES

FIGURE PAGE

ABBREVIATIONS AND ACRONYMS

AADTT	Annual Average Daily Truck Traffic
AASHTO	American Association of State Highway and Transportation Officials
EICM	Enhanced Integrated Climate Model
ESAL	Equivalent Single Axle Load
FDOT	Florida Department of Transportation
GMSL	Global Mean Sea Level
GWT	Groundwater Table
IPCC	Intergovernmental Panel on Climate Change
IRI	International Roughness Index
LTPP	Long-Term Pavement Performance
ME	Mechanistic-Empirical
MEPDG	Mechanistic-Empirical Design Guideline
MERRA	Modern-Era Retrospective analysis for Research and Applications
NOAA	National Oceanic and Atmospheric Administration
SLR	Sea-Level Rise
SN	Structural Number
SWCC	Soil-Water Characteristic Curves
UMAT	User Material

CHAPTER 1: INTRODUCTION

1.1 Background

Climate change is a global phenomenon manifesting worldwide, creating major problems, such as increasing average temperatures, changing storm patterns, and sea-level rise (SLR) (1, 2). Thermal expansion, glacier melting, and land water storage changes are the considered factors for the SLR. The Intergovernmental Panel on Climate Change (IPCC) report (3) projects the global mean sea level (GMSL) to rise by 17 inches (0.43 m) under low greenhouse gas emissions scenario and by 33 inches (0.84 m) under high emissions scenario by 2100. The National Oceanic and Atmospheric Administration (NOAA), likewise, predicts a GMSL rise in a range of 8.4 inches (0.21 m) to 79.2 inches (2.0 m) by the end of this century (4).

The evident effects of sea-level rise are increased flooding, coastal inundation, and rising groundwater levels (5). More than three-fourths of Florida's population is living in coastal communities. They produce more than $750 billion in goods and services (6). Thus, it is crucial to preserve its coastal infrastructure that is becoming vulnerable to the impacts of sea-level rise. Coastal cities monitor their coastal highways for increasing risk of surface flooding, coastal inundation, and erosion; however, rising groundwater table (GWT) levels can also affect roadways and infrastructure in inland areas (7).

Flexible pavement structures are supported by unbound layers that are highly sensitive to moisture. Increases in groundwater table elevation reduce the

unsaturated/vadose zone thicknesses (8) and threaten highways, underground utilities, and foundations in the coastal cities (9, 10). Furthermore, the rise of the groundwater table level reduces the normal and shear strength of the subgrade along with unbound pavement layers such as base and subbase. Therefore, anticipated changes in groundwater levels caused by sea-level rise can decrease the structural capacity of existing roads and accelerate their deterioration.

Several studies investigated the impacts of GWT rise on pavement performance around the world. As stated by Patel et al. (11), it is found that road failure is a common problem in the Shirpur region of India due to having high groundwater table levels. Additionally, the Institute of Public Works Engineering Australia handbook (12) depicts that road pavement's life span decreases considerably when GWT escalates to within 6 feet of the surface. Moreover, Roshani (13) predicts that by 2070, the groundwater level will be less than 3.3 feet below the pavement surface, and 32% of roadways along the Gold Coast will become vulnerable in Australia. Likewise, Knott et al. (14) assessed that SLR-induced groundwater level rise decreases the life expectancy of coastal pavement structures in New Hampshire by 50% from fatigue-cracking failure and up to 90% from rutting failure in case groundwater moves into pavement base layers. Feng et al. (15) also pointed out that the rise of GWT increases the maximum vertical displacement of the pavement surface.

1.2 Research Gaps

Considering the low elevation and porous geography of the Florida coastline as well as inland counties, the majority of its flexible pavement structures are becoming

damage-susceptible to high groundwater table's effects. Nevertheless, the impacts of SLR-induced high groundwater table on flexible pavement longevity have not yet been investigated in Florida. Evaluating the flexible pavement structural performance with high groundwater table conditions could aid in identifying future roadway vulnerabilities. Therefore, this evaluation can guide local legislators and agency officials for proactive actions to extend pavement longevity in the region.

The Florida Department of Transportation (FDOT) expressed a plan of using a mechanistic-empirical (ME) pavement analysis approach (16) in place of the empirical American Association of State Highway and Transportation Officials (AASHTO)'93 approach (17) in the future. However, there is a knowledge gap as there has not been any comparative analysis of Florida flexible pavement structures using both approaches. The AASHTO'93 method is based on AASHTO road tests observations so that it is empirical only. On the other hand, the ME method considers various inputs (material properties, climate, and traffic data) to predict pavement responses over pavement design life. It also evaluates pavement longevity in terms of pavement distresses, deterioration, and ride quality. Thus, analyzing the pavement structural performance with the ME approach can enrich the department knowledge to improve the resiliency of the roadway structures and can point out differences between empirical and ME methods.

Moreover, the mechanistic analysis approaches on flexible pavements' structural analysis do not consider the nonlinear (stress-dependent) behavior of base, subbase, and subgrade soils. Assigning a single resilient modulus value to entire unbound pavement layers neglects the variances created in both horizontal and vertical directions (18). These variances might influence the flexible pavement structural performance and the accuracy

of predicted pavement responses. Hence, there is a need to investigate stress-dependent material nonlinearity on Florida pavement structural performance.

1.3 Research Objectives

This research evaluates the impacts of sea-level rise induced-high groundwater table (GWT) on Florida flexible pavement structural performance. The main objectives are:

1. Determine the longevity of typical Florida flexible pavement structures with rising groundwater table conditions by conducting empirical and mechanistic-empirical (ME) pavement damage analyses.
2. Assess how pavement performance parameters (roughness, fatigue cracking, and rutting) would be affected by rising groundwater table (GWT) levels in Florida and determine predicted causes of pavement failures under different GWT conditions.
3. Compare the analysis results from the existing empirical method with the mechanistic-empirical (ME) method to determine if the two approaches predict the reduction in pavement service life consistently.
4. Evaluate the influence of nonlinear stress-dependent material behavior on critical pavement responses by comparing linear elastic pavement analysis with finite element method-based nonlinear analysis.

1.4 Thesis Outline

This thesis is organized into five chapters. The first chapter provides an introduction to the problem, research gaps, and thesis objectives. Chapter two presents the literature review as it relates to Florida sea-level rise and groundwater table level projections. Additionally, the empirical, mechanistic-empirical, and mechanistic flexible pavement structural analysis approaches are explained in Chapter two. Chapter three elaborates the methodology used to conduct this research while giving a detailed breakdown of organized step-by-step ana approaches. Chapter four contains the results and discussion addressing the objectives of this thesis. Chapter five presents the conclusion, where main findings from the results are revisited, recommendations for future work, and the limitations (Figure 1).

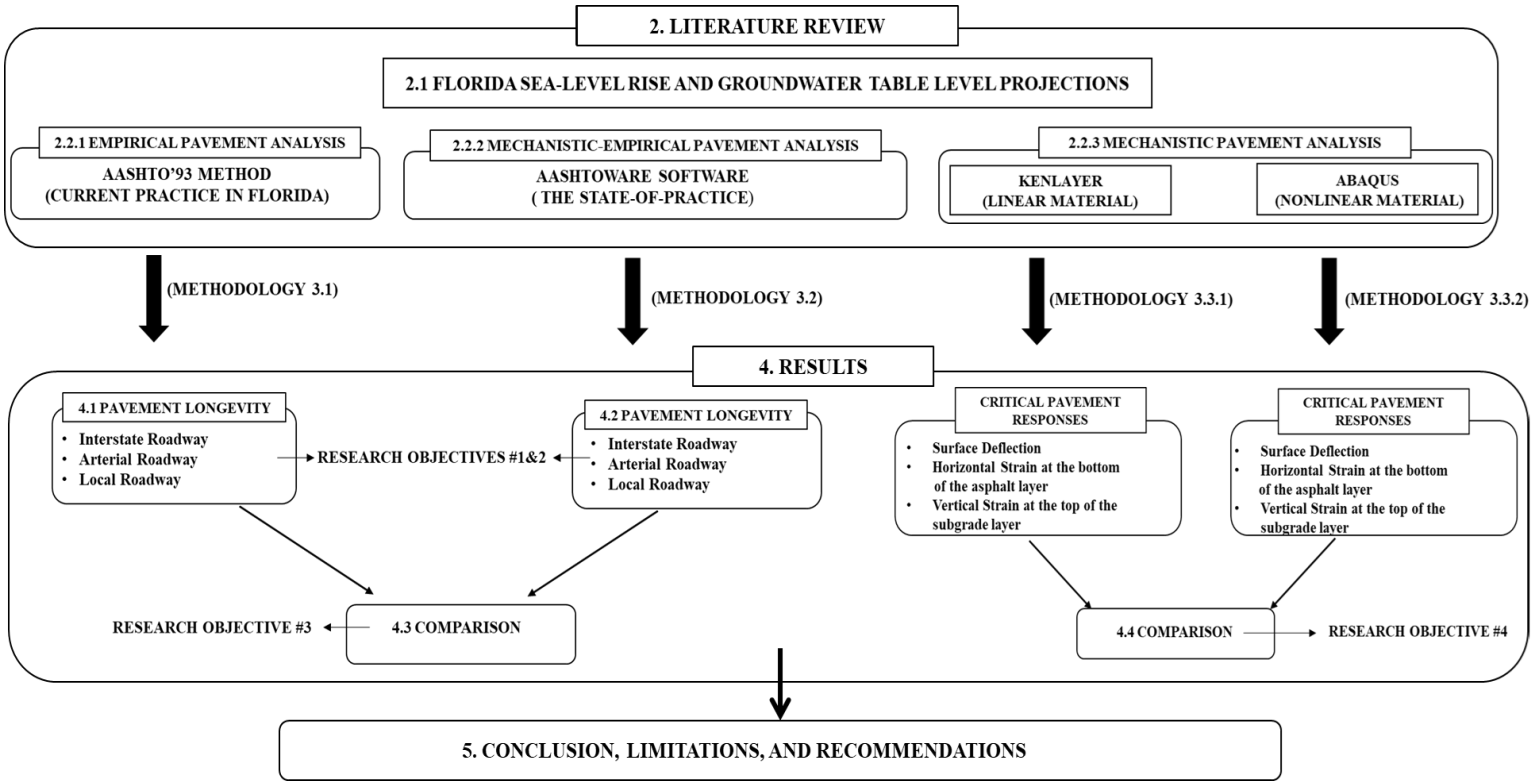

Figure 1: Thesis Outline

CHAPTER 2: LITERATURE REVIEW

2.1 Florida Sea Level Rise (SLR) and Groundwater Table (GWT) Level Projections

Sea Level Rise (SLR) is a global concern observed worldwide as consequences associated with anthropogenic forcing and climate change. Reports indicate that the global mean sea level (GMSL) has elevated about 8 inches since the beginning of the 20th century (19, 20) and is rising at an accelerating rate (3). Likewise, the sea level around Miami has been increased by about 4 inches since 1994 (21).

Nevertheless, Florida's sea-level rise rate has been higher than the global average (22). It should be acknowledged that the local conditions might also create variances between the regional sea-level rise (SLR) projections and the global forecast. Therefore, the Southeast Florida Regional Climate Change Compact has been combining the experiences of federal agencies and the academic community since 2011 to determine local SLR predictions in order to guide future projects and strategies in this region. Thus, the 2019 Prediction (23) recommends using 50-year sea-level rise projections from NOAA High Curve for critical infrastructure and the NOAA Intermediate High Curve for the most infrastructure projects, plus the median of the IPCC High Emissions Scenario for low-risk projects. Hence, the relative sea level in Southeast Florida is forecasted to rise by 10 to 17 inches in the short term and up to 54 inches by 2070 (Table 1).

Table 1: Unified Sea Level Rise Projection nearby Key West, FL (Inches Relative to Mean Sea Level in the Year 2000) (Source: South Florida Regional Climate Change Compact (23))

Year	IPCC Median Global (inches)	NOAA Intermediate High (inches)	NOAA High (inches)
2030	8	12	14
2040	10	17	21
2060	17	31	41
2070	21	40	54
2100	33	74	73
2120	40	92	136

Rising sea levels cause the groundwater table in coastal areas to increase in order to adjust to the new conditions (24, 25, 26, 27). Studies recently conducted by Decker et al. (28) and Sukop et al.(29) point out that groundwater levels in the Southeast Florida coastal zones increased at the same rate as relative sea-level rise in the region. Florida International University Sea Level Rise Solution Center (30) investigated the potential implications of sea-level rise and changing rainfall for communities in Florida using Miami-Dade County as a case study and estimated the change in water table elevation in Miami-Dade County by 2069. This study used the median of the IPCC High Emissions Scenario as a low-SLR predictor and the NOAA High Curve scenario as a high-SLR predictor. The report depicts that high groundwater table levels will impact the majority of Miami-Dade County under both sea-level rise scenarios (Figure 2).

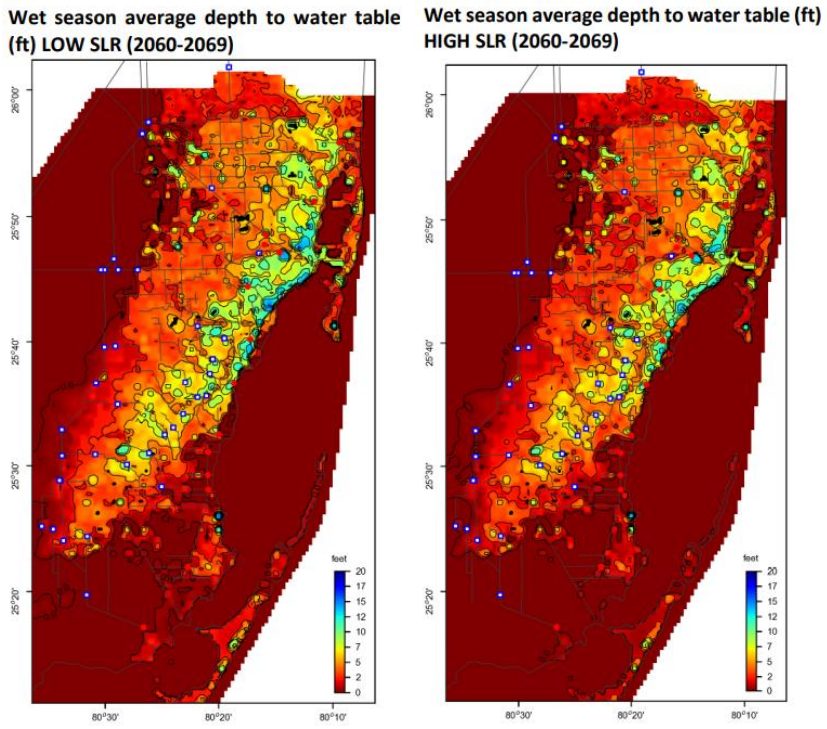

Figure 2: Miami-Dade County Predicted Average Groundwater Table Depth under LOW and HIGH SLR scenarios (Source: Obeysakara et al. (30))

Likewise, Rojali et al. (31) adopted the aforementioned maps (30) and used the Urban Miami Dade model to identify vulnerable roadway infrastructure that would be affected by the rising groundwater table levels. This study defined five vulnerability risk levels based on the predicted depth of the groundwater table. Risk level 1 showed the lowest risk condition for the roadway sections when the depth of the groundwater table is 5 ft or more beneath the surface. Risk level two represented slightly higher groundwater table condition ranges (3.5 ft to 5 ft depth). The groundwater depth range of 2.5 ft to 3.5 ft was labeled as moderate risk (level 3) for the roadways. Finally, the roadway structures were considered at the highest risks when the GWT is closer than 2.5 ft from the surface (Table 2).

Table 2: Predicted Risk Levels for Different Florida Roadway Classes (Source: Rojali et al. (31))

Risk Level	Depth to Groundwater Table	Interstate		Arterial		Collector & Local	
		Low SLR	High SLR	Low SLR	High SLR	Low SLR	High SLR
4&5	Less than 2.5 ft	0	4%	4%	14%	4%	15%
3	Less than 3.5 ft	22%	31%	33%	49%	32%	47%
2	Less than 5 ft	42%	49%	60%	69%	58%	65%
1	More than 5 ft	0	51%	40%	31%	42%	35%

This study shows that under High SLR scenarios, 49% of the Miami-Dade County interstate roadway sections, 69% of the arterial, and 65% of the local roadways would face 5 ft or higher groundwater table levels. Taking everything into account, the impacts of rising groundwater table levels on Florida pavement structural performance must be investigated.

2.2 Flexible Pavement Structural Analysis Approaches

2.2.1 Empirical Analysis Approach (AASHTO'93 Method)

The empirical pavement analysis approach is based solely on the equations developed from field performance data obtained at the American Association of State Highway Officials (AASHTO) Road Test in Ottawa, Illinois (17). The AASHTO 1993 approach has been regularly used around the world for decades due to its simplicity to utilize. The aim of the AASHTO equation (Equation 1) in the pavement thickness design process is to determine the required structural number (SN), which is the strength of the pavement that must be constructed to carry the mixed vehicle loads over the roadbed soil while providing adequate serviceability throughout the design period (32). The AASHTO equation (Equation 1) can also be used to predict the amount of traffic that can be

sustained before the pavement deteriorates to some selected terminal level of serviceability.

$$\log_{10}(W_{18}) = Z_R \times S_O + 9.36 \times \log_{10}(SN+1) - 0.20 + \frac{\log_{10}(\frac{\Delta PSI}{4.2-1.5})}{0.4 + \frac{1094}{(SN+1)^{5.19}}}$$

$$+2.32 \times \log_{10}(M_R) - 8.07$$

Equation 1

where:

$W_{18} =$ accumulated 18-kip (80 kN) Equivalent Single Axle Loads (ESAL) over the life of the project

$Z_R =$ standard normal deviate

$S_O =$ combined standard error of the traffic prediction and performance prediction

$\Delta PSI =$ initial serviceability index (P_O) minus terminal serviceability index (P_T)

SN = structural number

$M_R =$ resilient modulus (psi)

The cumulative traffic loading over the design period of the pavement structure (W_{18}) is determined by converting each predicted axle load from the mixed traffic flow into an equivalent number of 18,000 lb. single axle loading (ESAL). Another component of the empirical design method is determining the representative resilient modulus of the underlying subgrade materials (M_R). The designer can either apply the laboratory testing

results of representative samples of subgrade materials directly or use assumed resilient modulus (M_R) values based on soil classification and anticipated drainage conditions in the selected location (33). Moreover, reliability is defined as the probability of achieving the expected design life for the chosen facility that is not the same for all highway functional classes. The value of (Z_R) is the corresponding reliability value converted into a logarithmic form for calculation purposes (32). The designer should also select the deterioration rate in terms of loss of serviceability (ΔPSI) for the project and the combined standard error (S_O) in percentages to consider traffic load prediction variabilities.

In the AASHTO'93 empirical approach, the structural number of pavement cross-sections is computed using the layers above the subgrade. It is associated with pavement layer thicknesses, structural coefficients, and drainage conditions, as shown in Equation 2.

$$SN = (a_1 \times D_1) + (a_2 \times D_2 \times m_2) + (a_3 \times D_3 \times m_3) \quad \text{Equation 2}$$

where:

SN = structural number

$a_1, a_2, a_3 =$ structural layer coefficients of the surface, base, and subbase layers, respectively

$m_2, m_3 =$ layer drainage coefficients of the base, and subbase layers, respectively

D_N = layer thickness in inches of the Nth layer

The structural layer coefficients for each layer can be estimated using the state guidelines, and the structural number of existing roadways can be calculated. Then, the amount of traffic that selected pavement sections are able to sustain before reaching the terminal level of serviceability can be predicted using the AASHTO equation (Equation 1).

Considering the fact that the AASHTO'93 equation uses the subgrade soil resilient modulus (M_R) input, any moisture-related strength loss within the layer could impact the performance predictions of the pavement structures. The Florida Department of Transportation (FDOT) flexible pavement design manual (32) considers the clearance between the groundwater table and base layer critical for good pavement performance. The manual defines a minimum 3ft clearance as an optimum moisture condition. The FDOT (32) also requires reducing the design subgrade resilient modulus (M_R) by 25% when the base clearance is between 2 ft and 3ft and by 50% in the case of the clearance is between 1ft and 2 ft based on the Ping and Ling (34) study. Therefore, this empirical approach can be efficient in investigating the differences in the structural capacity in terms of the allowable amount of traffic for this particular problem of rising groundwater levels. The empirical pavement evaluation methodology will be explained in Chapter 3.1.

2.2.2 Mechanistic-Empirical Analysis Approach (AASHTOWare Pavement ME Software)

The objective of the mechanistic-empirical approach is stated as "providing the pavement designer a state-of-the-practice analysis tool for the design and analysis of new

and rehabilitated pavement structures based on mechanistic-empirical principles" (16). It unites two approaches. The one is a mechanistic approach that uses fundamental knowledge about how critical pavement responses (deflections, stresses, and strains) change through pavement structure under traffic and climatic loading conditions. It is combined with an empirical approach that defines relationships about the damage that is going to result from those stresses, strains, and previous conditions to predict how pavement will react over time (Figure 3).

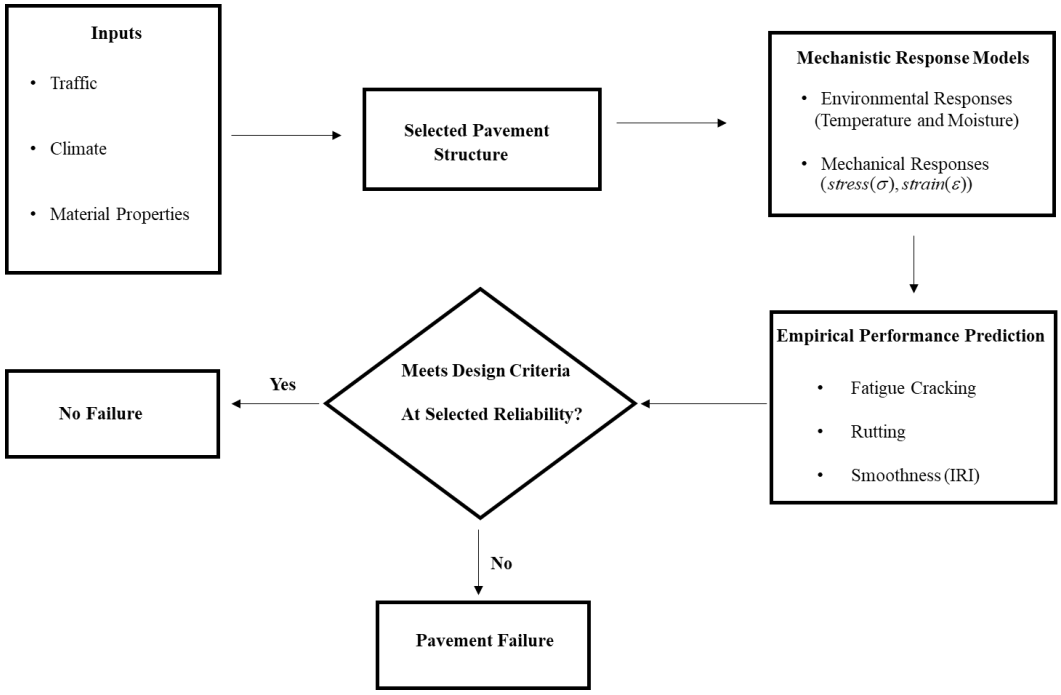

Figure 3: The Steps of Mechanistic-Empirical Pavement Analysis (35)

The AASHTOWare pavement structural analysis software requires inputs related to the climate, traffic loading, and material properties for the selected pavement cross-section. Once the failure criteria of the roadway are also assigned, pavements' structural performance can be evaluated. Mechanistic-empirical design software runs the Enhanced

Integrated Climate Model (EICM) that predicts the environmental responses that include moisture and heat distribution throughout the pavement structure. Then, mechanistic models within the software calculate the structural responses (stress, strain, and deflection) at the critical pavement response locations. Calculated pavement responses are then used as an input within the empirical performance models that link these responses to predict pavement distresses such as rutting, fatigue cracking, and pavement roughness. The AASHTOWare software uses empirical performance models that were nationally calibrated using several pavement test sections all around the United States.

The AASHTOWare software provides a significant advantage to the purpose of this study. The software utilizes detailed climatic data, unlike the AASHTO'93 method, to predict pavement distresses and longevity more accurately. The Enhanced Integrated Climatic Model (EICM) within the software uses hourly weather data (air temperature, precipitation, wind speed, percentage of sunshine, and relative humidity) along with the groundwater depth as inputs. Then, it reproduces pavement temperature, sublayer moisture profiles, and resilient modulus adjustment factors (Fenv) throughout the design life of a pavement structure. Equation 3 expresses the resilient modulus (M_R) at any time or position as follows:

$$M_R = F_{env} x\, M_{Ropt} \qquad \text{Equation 3}$$

M_{Ropt} is the resilient modulus at optimum conditions in a unit of psi.

EICM models the adjustment factor F_{env} as a function of soil moisture using the following model presented in Equation 4.

$$F_{env} = 10^{\left(a+\frac{b-a}{1+EXP(\ln(-b/a)+k_m.(S-S_{opt}))}\right)}$$ Equation 4

where:

a= minimum of log (M_R/M_{Ropt}),

b = maximum of log (M_R/M_{Ropt}),

k_m = regression parameter,

(S-S_{opt}) = variation in the degree of saturation expressed in decimals.

The mechanistic-empirical design guideline (MEPDG) provides the values of a, b, and for both coarse-grained and fine-grained materials to be used in Equation 4 (16). The EICM model predicts the degree of saturation parameter (S) from the soil matric suction by using the soil-water characteristic curves (SWCCs) relationship model (36) and Witzcak et al. (37)'s correlations as explained in Appendix B.

Moisture-related changes within the base, subbase and subgrade layers that constitute a large portion of the pavement structure could contribute to distress and failures. Since the mechanistic-empirical software adjusts the resilient modulus of unbound layers according to their moisture levels, it is an effective tool to evaluate pavement longevity with the sea level rise-induced rising groundwater table level problem. The evaluation methodology will be explained for this method in Chapter 3.2.

2.2.3 Mechanistic Analysis Approaches (Linear Multi-layered Elastic Analysis and Finite Element Models)

There are specific mechanistic analysis approaches on flexible pavements' structural analysis. To illustrate, two of the major approaches are the linear multi-layered elastic analyses and the finite element modeling method. Mechanistic pavement analysis methods utilize engineering mechanics theories to apply traffic loading to pavement structural performance.

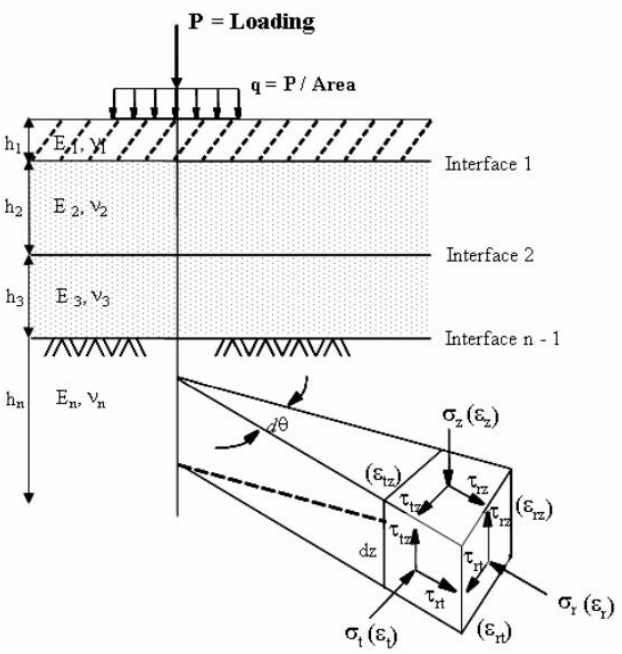

Figure 4: Linear Multi-layered Elastic Pavement Structure for Axisymmetric Analysis (38)

To be able to conduct multi-layer elastic analysis, pavement engineers must determine the modulus of elasticity ($E_1, E_2, ..E_n$), Poisson ratio ($v_1, v_2, ..v_n$), and

thicknesses ($h_1, h_2, ..h_n$) of selected layers. The magnitude of total force (P) is generally chosen as 18-kip (80kN) loading representing an equivalent single axle load (ESAL).

Mechanistic analysis methods cannot be used solely to design pavement sections. However, these approaches can compute deflections, stresses, and strains in the designed pavement structure resulting from the application of wheel loads, as shown in Figure 4. Pavement failure (i.e., rutting and fatigue cracking) are linked with predicted critical pavement responses. Critical pavement responses can be stated as (1) the maximum horizontal tensile strain at the bottom of the asphalt layer, (2) vertical compressive strains at the top of the base/subgrade layers, and (3) pavement surface deflection (39).

Although multi-layer mechanistic analysis tools assume each pavement structural layer's being homogeneous, isotropic, and linearly elastic, they have been easily implemented and widely accepted. A few researchers (14, 40) have used the KENLAYER to investigate the impacts of sea-level rise on flexible pavement performance. To implement the influence of moisture on the unbound base, subbase, and subgrade layers, the elasticity of modulus of saturated materials was reduced empirically (up to 50%) in these analyses. For the purpose of this study, the existing FDOT resilient modulus adjustment factors were used to implement the impacts of rising groundwater table levels.

The finite element method utilizes numerical analysis techniques to provide approximate solutions for a wide range of engineering problems. ABAQUS is the most commonly used finite-element method-based software that can be applied to linear and nonlinear pavement analysis (38). Unlike the linear multi-layered elastic analysis

approach, the ABAQUS software provides an interface to define any particular material's mechanical behavior model with a user material (UMAT) subroutine written in FORTRAN language. Figure 5 demonstrates the axisymmetric typical flexible pavement model created on ABAQUS software and the user material interface of the software.

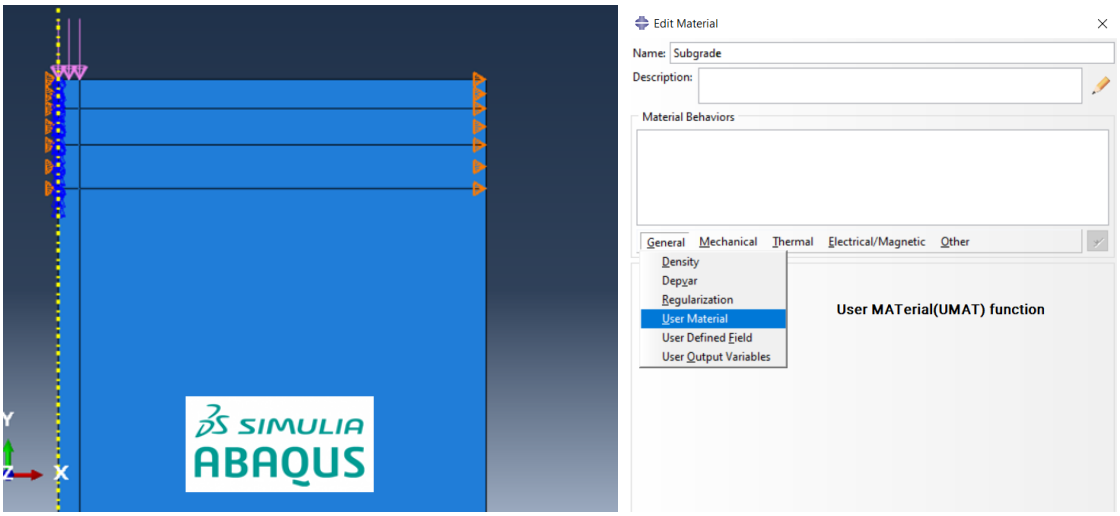

Figure 5: Typical ABAQUS Pavement Structure for Axisymmetric Analysis and ABAQUS User Material Interface

Unbound granular materials and subgrade soil resilient modulus are known to be dependent on the stress state that each pavement layer is subjected. The modulus value changes in horizontal and vertical directions because the stress levels show variances within a layer. The association of Australian and New Zealand road transport and traffic agencies (41) already considers the stress-dependent variances within the granular base and subbase layers. In fact, it divides pavement layers into five sublayers and assigns decreasing vertical resilient modulus values to each layer moving from top to bottom corresponding to the decreasing vertical stress levels at which they operate. To conduct pavement mechanistic analysis more accurately, therefore, layer modulus distributions

should be determined by models that consider material resilient modulus as a function of stress states. Some models (42, 43, 44) that incorporated stress state-effect on the resilient modulus are shown below (Equation 5 to Equation 7).

$$M_R = k_1 \times (\theta)^{k_2}$$ Equation 5

$$M_R = k_1 \times p_a \times \left(\frac{I_1}{p_a}\right)^{k_2} \times \left(\frac{\tau_{oct}}{p_a}\right)^{k_3}$$ Equation 6

$$M_R = k_1 \times p_a \times \left(\frac{I_1}{p_a}\right)^{k_2} \times \left(\frac{\tau_{oct}}{p_a}+1\right)^{k_3}$$ Equation 7

where:

$M_R =$ resilient modulus (psi); k_1, k_2, k_3 = regression constants; θ = bulk stress (psi); I_1 = first stress invariant (psi) ; τ_{oct} = octahedral shear stress (psi), and p_a =atmospheric pressure (14.7 psi)

Equation 7 was utilized to characterize the stress-dependent behavior of both fine-grained subgrade soils and unbound aggregates and programmed using the UMAT subroutine of the ABAQUS software. Furthermore, a resilient modulus adjustment factor was included in this stress-dependent material model to implement Florida requirements for rising groundwater table levels in as shown in Equation 8.

$$M_R = f_1 \times k_1 \times p_a \times \left(\frac{I_1}{p_a} \right)^{k_2} \times \left(\frac{\tau_{oct}}{p_a} + 1 \right)^{k_3} \quad \text{Equation 8}$$

f_1 = resilient modulus adjustment factor (1.0 for optimum groundwater condition, 0.75 or 0.50 for higher groundwater table conditions).

In ABAQUS, nonlinear elasticity material behavior needs to be rewritten as a strain-stress relationship. Therefore, the elastic material matrix can be expressed as (Equation 9) converting generalized Hooke's law to represent nonlinear mechanical behavior.

$$D = \frac{E}{(1+v)(1-2v)} \begin{bmatrix} 1-v & v & v & 0 & 0 & 0 \\ v & 1-v & v & 0 & 0 & 0 \\ v & v & 1-v & 0 & 0 & 0 \\ 0 & 0 & 0 & \frac{1-2v}{2} & 0 & 0 \\ 0 & 0 & 0 & 0 & \frac{1-2v}{2} & 0 \\ 0 & 0 & 0 & 0 & 0 & \frac{1-2v}{2} \end{bmatrix} \quad \text{Equation 9}$$

where: D= Elasticity Matrix; E= Young's modulus; and ν = Poisson's ratio.

The researchers (45, 46, 47) substituted the stress-dependent resilient modulus models for Young's modulus in previous studies to update the elastic material matrix within each element accordingly. Therefore, Equation 8 was utilized for this study. The stress-dependent behavior of unbound base, subbase, and subgrade soils was incorporated into the finite-element solution through this implementation. Consequently, resilient modulus properties varying with both horizontal and vertical distance in each pavement layer were predicted as a function of stress levels.

Once a nonlinear pavement model was created using the UMAT subroutine, a single wheel load will be applied to the multi-layered pavement structure model to determine critical pavement responses similarly to the linear elastic analysis. Then, Chapter 3.3 will explain the analysis methodologies using linear and nonlinear mechanistic analysis to evaluate the influence of material stress-dependent nonlinearity on critical pavement responses in Florida.

CHAPTER 3: METHODOLOGY AND DATA

To fulfill the first objective of this thesis, which was to determine the longevity of typical Florida pavement structures with rising groundwater table conditions, two different analytical methods, the Mechanistic-Empirical (ME) design software (AASHTOWare) and the existing FDOT empirical method, were utilized. Florida roadways were categorized into three classes which are interstate roadways (IR), arterial roadways (AR), and local roadways (LR). Then, four potential groundwater table levels of interest were identified considering sea-level rise projections in the region as GWL1, GWL2, GWL3, and GWL4, representing 5 ft, 3,5 ft, 2.5 ft, and 1.5 ft groundwater table depth, respectively. Typical pavement cross-sections were determined using the existing Florida flexible pavement design manual (32) and the AASHTO Equation (Equation 1). Resilient modulus inputs were adjusted corresponded to the groundwater table for the empirical damage analysis as current Florida requirements. On the other hand, AASHTOWare software reproduced the moisture profiles of unbound layers and adjusted resilient modulus values through the design life of pavement structures. Analysis results were recorded to fulfill the second objective of the thesis, which was to assess how pavement performance parameters (roughness, fatigue cracking, and rutting) would be affected by rising groundwater table (GWT) levels in Florida and to determine predicted causes of pavement failures under different GWT conditions. The pavement longevity outputs from the empirical analysis and AASHTOWare software were compared to fulfill the third objective of this thesis, which was to determine if the two pavement analyses predicted pavement longevity loss in a consistent manner.

To fulfill the fourth objective of this thesis, which was to evaluate the influence of stress-dependent material nonlinearity on critical pavement responses, ABAQUS and KENLAYER software were used. UMAT subroutine of ABAQUS software was used to develop stress-dependent nonlinear material models for the base, subbase, and subgrade layers. Typical pavement cross-sections for each roadway class and groundwater table levels (GWL1, GWL2, GWL3, and GWL4) were kept the same for both analyses. Subgrade resilient modulus inputs were adjusted corresponded to the groundwater table following the current Florida requirements for both analyses. A wheel load was selected constant at 80 psi tire pressure with a contact radius (R) of 6 inches. First, the critical pavement responses, vertical deflection on the asphalt surface, horizontal tensile strain at the bottom of the asphalt layer, and vertical compressive strain on the top of the subgrade layer were predicted for the optimum groundwater table condition (GWL1). Pavement structures were reevaluated, and critical pavement responses under rising groundwater level conditions were recorded. Finally, analysis results for each groundwater level were compared.

3.1 Empirical Pavement Structural Analysis

Figure 6 describes the empirical pavement analysis flowchart to fulfill the first two objectives of the thesis.

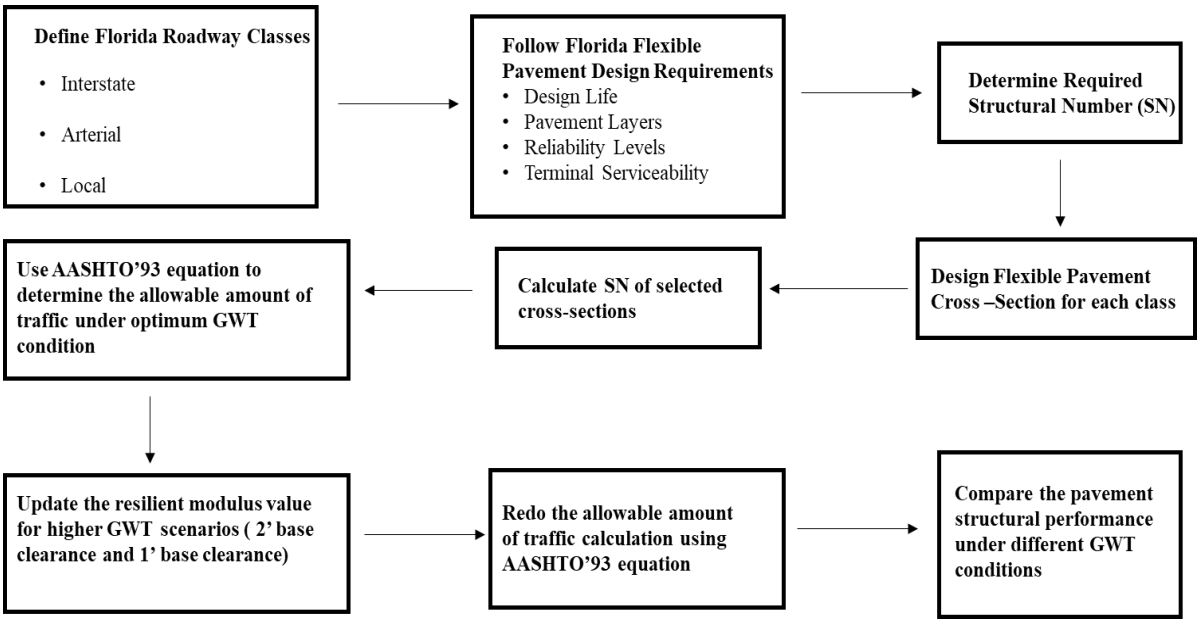

Figure 6: The Empirical Pavement Structural Performance Analysis Flowchart

3.1.1 Empirical Pavement Analysis Inputs

Structural analysis of flexible pavement requires input parameters such as design period (years), reliability level (%), combined standard error (unitless), and serviceability index (unitless). The Florida flexible pavement design manual (32) provides constant input values to be used in the AASHTO equation (Equation 1).

Table 3: Empirical Flexible Pavement Analysis Inputs (Source: FDOT (32))

Parameter	Value
Design Life (years)	20
Standard Deviation (S_O)	0.45
Initial Serviceability (P_O)	4.2
Terminal Serviceability (P_T)	2.5
Change in Serviceability (ΔPSI)	1.7

For the purpose of this analysis, Florida roads were categorized into Interstate Roads (IR), Arterial Roads (AR), and Local Roads (LR) based on their traffic and reliability levels. IR included limited access roadway sections, AR contained both urban and rural arterial roadways, and LR represented the collectors and low volume roadway sections. Therefore, 95%, 85%, and 80% were selected reliability levels for IR, AR, and LR, respectively.

Table 4: Reliability (%R) for Different Roadway Facilities (Source: FDOT (32))

Facility	Reliability
Limited Access	80% - 95%
Urban Arterials	80% - 90%
Rural Arterials	75% - 90%
Collectors	75% - 80%

Table 5 depicts Florida traffic levels from the lowest to the highest (A to E) in terms of Design Equivalent Single Axle Loads ($ESAL_D$) ranges. While an ESAL load represents an 18,000 lb single-axle loading, the mixed flow of traffic flow is converted into ESAL to determine accumulated traffic loadings over a pavement design period.

Table 5: Florida Traffic Levels (Source: FDOT (32))

Design Traffic Range (Million ESALs)	Traffic Level
< 0.3	A
0.3 to < 3.0	B
3 to < 10	C
10 to < 30	D
>= 30	E

Traffic loading that typical interstate roadway pavement structures face during their design life is typically in traffic Level D. Arterial roadways operate less traffic loading daily than IR; thus, traffic level C was assumed for the design purposes. Since local roadway pavement structures withstand the lower traffic, traffic level B was considered for its structural design. Selected traffic levels for each roadway class show consistency with an existing study (48). Therefore, Table 6 depicts traffic inputs were selected for IR, AR, and LR, respectively.

Table 6: Traffic Inputs for Selected Roadway Classes

Roadway Class	Design Traffic (Million ESALs)
Interstate Roads (IR)	28.7
Arterial Roads (AR)	9.0
Local Roads (LR)	1.5

The FDOT flexible pavement design manual (32) defines groundwater table depth as a critical parameter for good pavement performance. If base clearance, the distance from the bottom of the base layer to the groundwater table level, is 3 ft or more, the pavement structure is assumed to be at optimum moisture condition. However, the pavement designer must reduce the design resilient modulus by up to 50% when the base clearance is lower than 3 ft.

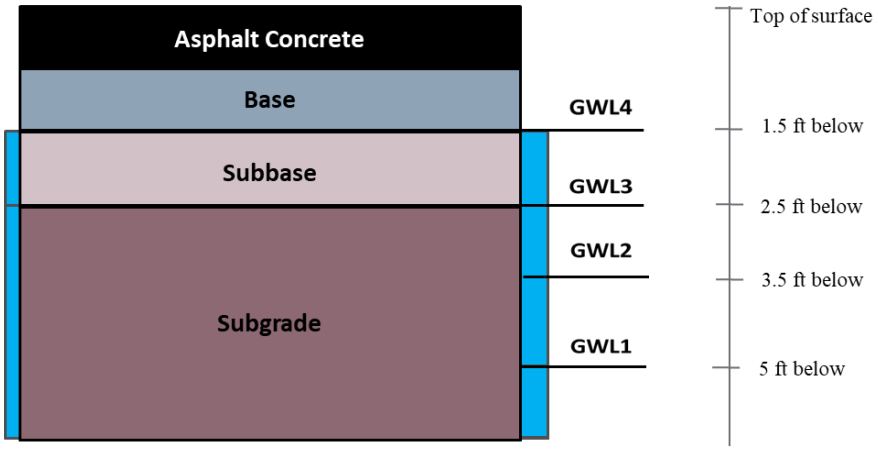

Figure 7: Typical Florida Pavement Structure with Selected Groundwater Table Levels

Figure 7 shows the typical pavement structure with 4 GWT level conditions that were defined for the purpose of empirical design analysis. First of all, the pavement structure with 5 ft groundwater depth (GWL1) was selected as the control section. Considering the sea-level rise projections for the region, 3.5 ft (GWL2), 2.5 ft (GWL3), and 1.5ft (GWL4) groundwater table depth conditions were selected. Thus, subgrade resilient modulus must be decreased by 25% for the GWL2 condition and 50% for GWL3 and GWL4 conditions for the analysis.

3.1.2 Empirical Analysis Pavement Structure Inputs and Selected Pavement Cross-Sections

Resilient modulus was assumed to be 8,000 psi based on typical soil conditions in Florida. The Florida flexible pavement design guideline requires having LBR40 stabilized subgrade when the subgrade resilient modulus is lower than 12,000 psi. The other structural layers selected for the cross-section design are the limerock (LBR100) base and SP-9.5 and SP-12.5 asphalt layers. The drainage factors for the base and

subbase layer were accepted as 1. Required structural numbers for each roadway class were determined by the AASHTO Equation (Equation 1).

Table 7: Required Structural Numbers for Selected Roadway Classes

Roadway Class	Required Structural Number (SN)
Interstate Roads (IR)	5.95
Arterial Roads (AR)	4.60
Local Roads (LR)	3.36

A structural layer coefficient (a_x) is assigned to each pavement layer to characterize "the relative ability of the material to function as a structural component of the pavement" in the empirical pavement analysis approach (17). Structural layer coefficients for selected pavement layers are shown in Table 8.

Table 8: Structural Layer Coefficients for Selected Pavement Layers (Source: FDOT (32))

Layer Type	Layer Coefficient (a_x) per inch
Superpave Type SP (SP-9.5,SP-12.5, SP-19)	0.44
Limerock (LBR100)	0.18
Type B Stabilization (LBR40)	0.08

Figure 8 presents the flexible pavement cross-sections for interstate roads, arterial roads, and local roads. Equation 2 was used to determine the structural numbers of the cross-sections. Thus, the structural number was calculated as 6.02 for typical interstate

roadway section, 4.74 for typical arterial roadway section, and 3.5 for typical local roadway section.

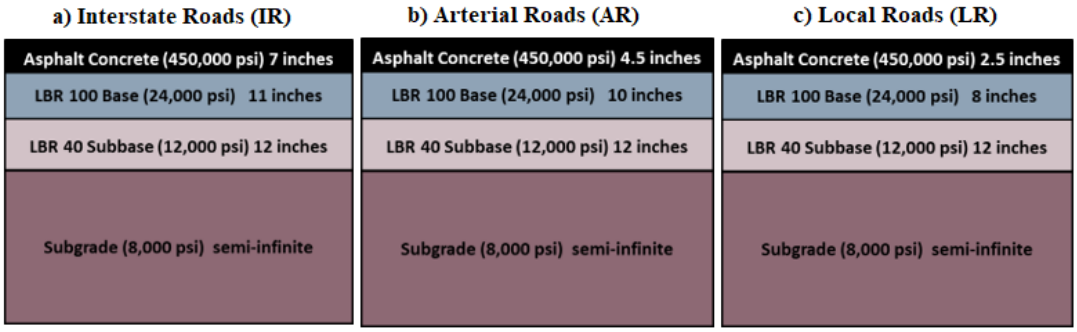

Figure 8: Pavement Cross-Sections for Interstate, Arterial, and Local Roads (From Left to Right)

3.2 AASHTOWare ME Pavement Structural Performance Analysis

Figure 9 describes the pavement analysis flowchart using AASHTOWare ME software to determine the pavement longevity of typical roadway structures from three roadway classifications (interstate, arterial, and local roadways).

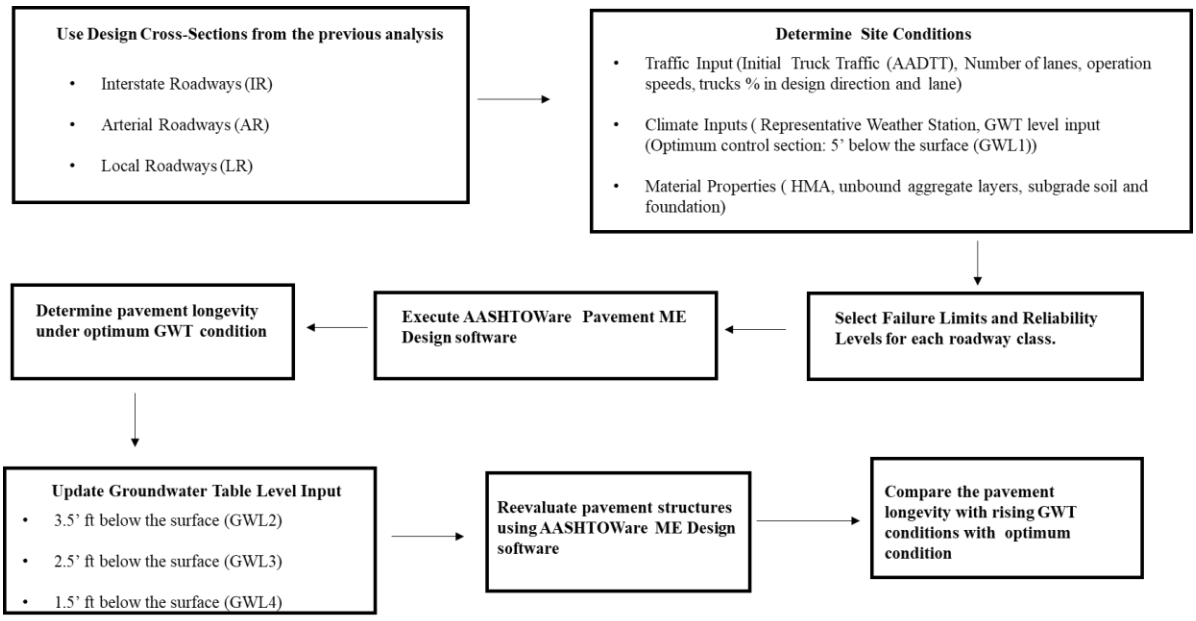

Figure 9: Mechanistic-Empirical Pavement Structural Analysis Flowchart

3.2.1 Mechanistic-Empirical (ME) Pavement Analysis Inputs

The AASHTOWare software requires several more inputs at a far greater degree of detail than the empirical analysis approach to accurately reflect site conditions. Therefore, traffic input data were selected from the available Florida Traffic Online website (49). Material properties were acquired from the long-term pavement performance (LTPP) database, and representative climate conditions were selected from the available MERRA (The Modern-Era Retrospective analysis for Research and Applications) database (50).

3.2.1.1 Design Life

The pavement design life was selected to be 20 years to compare the mechanistic-empirical analysis and the empirical analysis results.

3.2.1.2 Performance Criteria and Reliability

Pavement structural performance of each roadway class in terms of three performance criteria; roughness (controlled by International Roughness Index (IRI)), fatigue cracking (% cracks in lane area), and rutting (rut depth in inches) was determined running various mechanistic-empirical (ME) analysis with changing groundwater table levels. A failure occurred when the first of the three criteria reached failure limits throughout the 20-year design service life. Pavement distress limits for each roadway class were determined following the MEPDG (16). Table 9 depicts the pavement distress thresholds for the selected roadway classes. For the purpose of comparison analysis,

reliability levels that were selected for empirical analysis were kept constant for mechanistic-empirical analysis (95%, 85%, and 80%, for IR, AR, and LR, respectively).

Table 9: The Mechanistic-Empirical (ME) Pavement Analysis Pavement Failure Criteria Inputs for Three Roadway Classes

Distress Type	Interstate Roadway	Arterial Roadway	Local Roadway
Terminal IRI (in/mile)	172.00	172.00	172.00
Rutting - total pavement (in)	0.40	0.50	0.65
AC bottom-up fatigue cracking (% lane area)	10.00	20.00	35.00
AC top-down fatigue cracking (% lane area)	10.00	20.00	35.00
Rutting - AC only (in)	0.15	0.20	0.30

3.2.1.3 Traffic Input

The mechanistic-empirical analysis method necessitates comprehensive traffic design inputs, which are listed as "an initial two-way average annual daily truck traffic (AADTT), number of lanes in design direction, percent of trucks in design direction, percent of trucks in design lane, operational traffic speed, and traffic distribution by vehicle class" (16). Initial AADTT values of selected roadway classes were selected from data available at the Florida Traffic Online website (49). Representative truck traffic (AADTT) for two-way six-lane interstate roadway section (Turnpike) was 13,655 (Fig. 10a), for two-way three-lane arterial roadway segment (West Flagler Street) was 3276 (Fig. 10b), and two-way one-lane local roads (Riverland Road) were 343 (Fig. 10c).

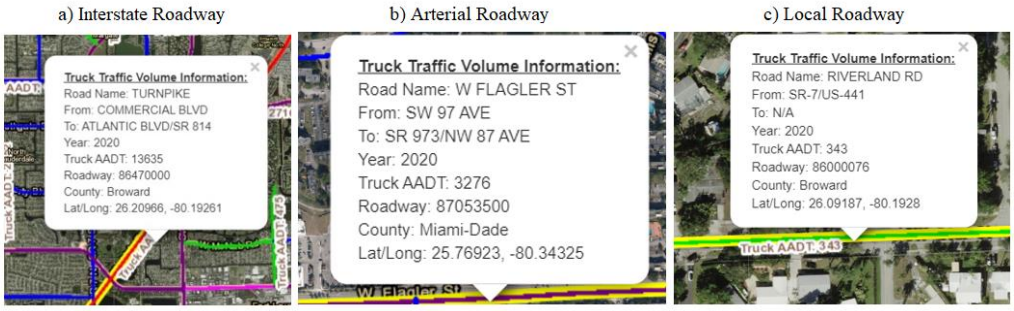

Figure 10: Representative Truck Traffic (AADTT) Values for a) Interstate Roadway Section, b) Arterial Roadway Section, c) Local Roadway Section

Operational speed values, 30, 45, and 70 mph for Riverland Road, West Flagler Street, and State Road 91, respectively, are derived from the posted speed limits in the selected roadway sections. Finally, the annual truck traffic growth rate was assumed to be 3%. The default values from the AASHTOWare software were used for other inputs regarding traffic distribution.

3.2.1.4 Climate Inputs

The Enhanced Integrated Climatic Model (EICM) within the software needs hourly weather data (air temperature, precipitation, wind speed, percentage of sunshine, and relative humidity) and the groundwater depth inputs. To get more accurate results, the weather station nearby the project area should be selected from the available MERRA (The Modern-Era Retrospective analysis for Research and Applications) database (50).

In this study, Florida Climate Station (ID: 129184) was selected for the ME analysis, and the summary of climate station inputs is shown in Figure 11.

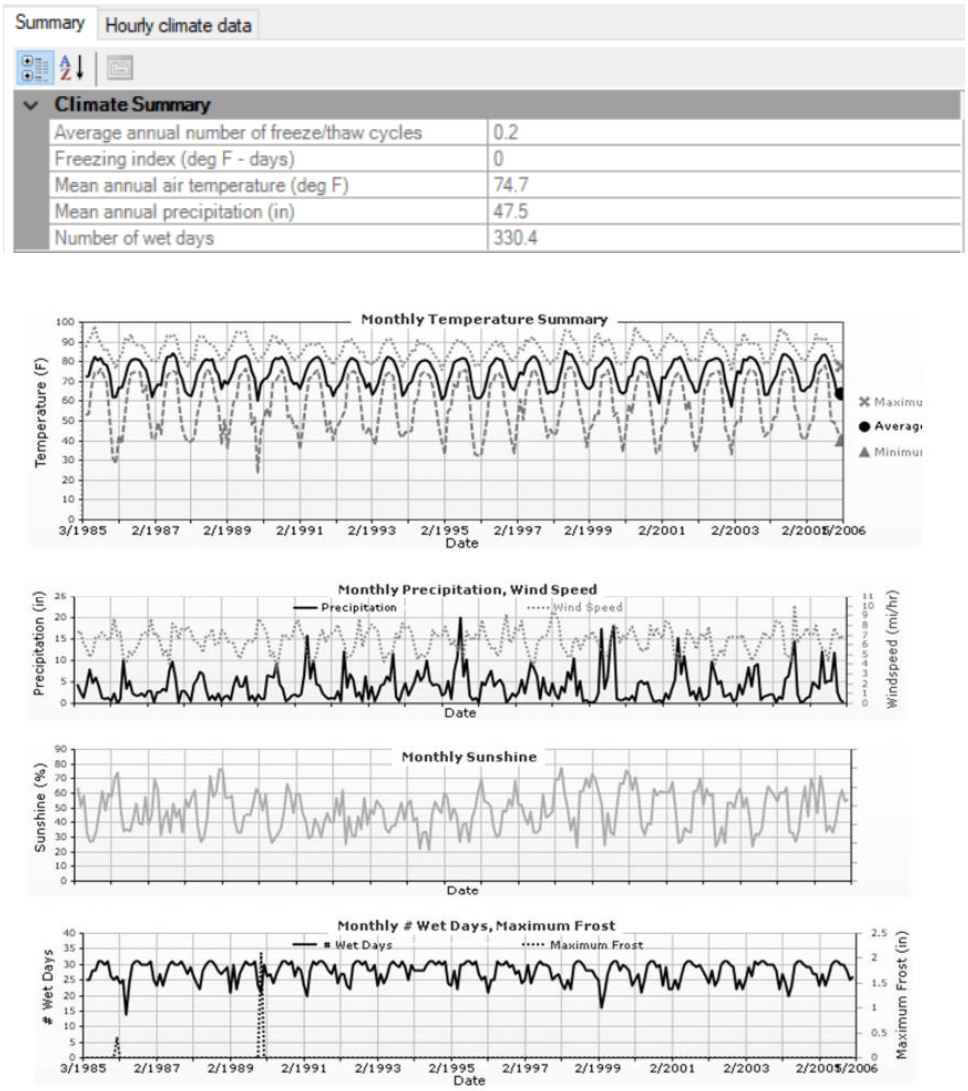

Figure 11: The Summary of Monthly Temperature, Precipitation, Wind Speed, Percentage of Sunshine, and the Number of Wet Days in the Selected Climate Station

3.2.2 Pavement Structure Inputs

The asphalt concrete material properties to utilize in mechanistic-empirical pavement analysis are shown in Table 10.

Table 10: Asphalt Layer Inputs for the Mechanistic-Empirical (ME) Pavement Analysis

Asphalt Layer	PG 76-22	PG 64-22
Poisson's ratio	0.35	
Effective binder content (%)	11.6	12
Air voids (%)	7	6.5
Maximum dry unit weight (pcf)	138	150
Aggregate parameter	0.329	0.379
Reference temperature (°F)	70	
Thermal conductivity (BTU/hr-ft-°F)	0.67	
Heat capacity (BTU/lb-°F)	0.23	
Asphalt content by weight %	4.5	
Dynamic modulus	Calculated by the software	

The long-term pavement performance (LTPP) program is managed by Federal Highway Administration (FHWA) and includes information collected from 2,509 pavement test sections all through the United States and Canada (51). For this study, the measured physical properties for unbound layer materials were obtained from the Florida sites available in the LTPP database (Table 11).

Table 11: Unbound Layers (Base, Subbase) and Subgrade Material Inputs for the Mechanistic-Empirical (ME) Pavement Analysis

MATERIAL		LIMEROCK (LBR100)	SUBBASE	SUBGRADE 1 (SILTY SAND)	SUBGRADE 2 (CLAYEY SAND)
Sieve Size (% Passing)	#200	16.2	13	32	13.5
	#80	30	95	57	35.4
	#40	43	99	85	47.3
	#10	59	100	97	65
	#4	66	100	100	75.3
	3/8-in.	73	100	100	84.3
	1/2-in.	77	100	100	87
	3/4-in.	83	100	100	91.8
	1-in.	90	100	100	94.8
	1 1/2-in.	98	100	100	95.9
	2-in.	98	100	100	98.2
	3 1/2-in.	100	100	100	100
Maximum dry unit weight (pcf)		118	123.5	119	123
Specific Gravity (Gs)		2.74	2.62	2.69	2.7
Water Content %		12	10.1	12	9
Liquid Limit (LL)		-	-	25	-
Plasticity Index (PI)		NP	NP	12	NP
Resilient Modulus (psi)		24000	12000	10717	7902
Poisson's ratio		0.40	0.40	0.45	0.45

The FHWA technical report (52) indicated using the bedrock as a part of pavement structure when it is supported by a compacted limerock embankment in Florida. In this study, IR and AR were assumed to be supported by a limerock embankment due to the importance of the projects. On the other hand, local roadways in Florida do not usually have limerock embankments underneath. Therefore, only the IR and AR pavement structures included semi-infinite bedrock support to represent the in-situ conditions more accurately. The inputs for the bedrock layer are shown in Table 12.

Table 12: Bedrock Material Input for the Mechanistic-Empirical (ME) Pavement Analysis

Layer thickness	Semi-Infinite
Poisson's ratio	0.15
Resilient Modulus (psi)	750,000
Unit weight (pcf)	140

3.2.3 Mechanistic-Empirical Analysis Pavement Cross Sections

Figure 12 summarizes the selected pavement structural cross-sections and groundwater table depth levels for the analysis. Four groundwater table depth inputs (GWL1, GWL2, GWL3, GWL4) are 5ft, 3.5 ft, 2.5ft, and 1.5 ft, respectively.

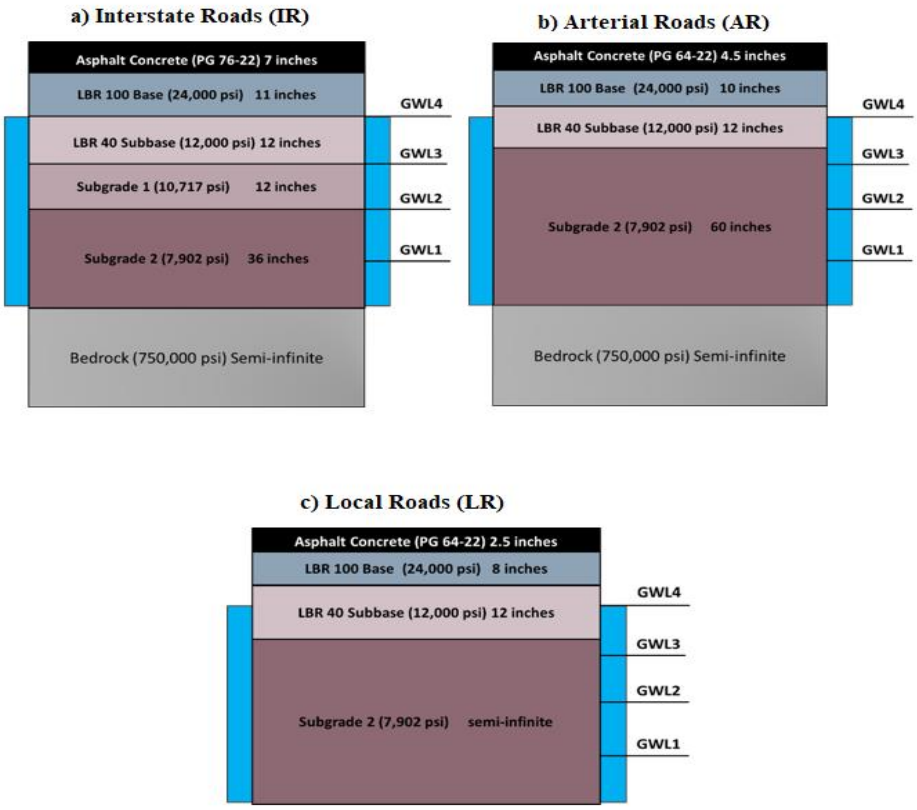

Figure 12: Pavement Cross-Sections with Selected Groundwater Table Levels for The Mechanistic-Empirical (ME) Pavement Analysis: a) IR Cross-Section, b) AR Cross-Section c) LR Cross-Section

3.3 Mechanistic Pavement Structural Analysis

3.3.1 Linear Multi-layered Elastic Pavement Analysis

Figure 13 illustrates the pavement analysis flowchart using KENLAYER software to evaluate the impacts of stress-dependent nonlinear material behavior on Florida pavement structure performance.

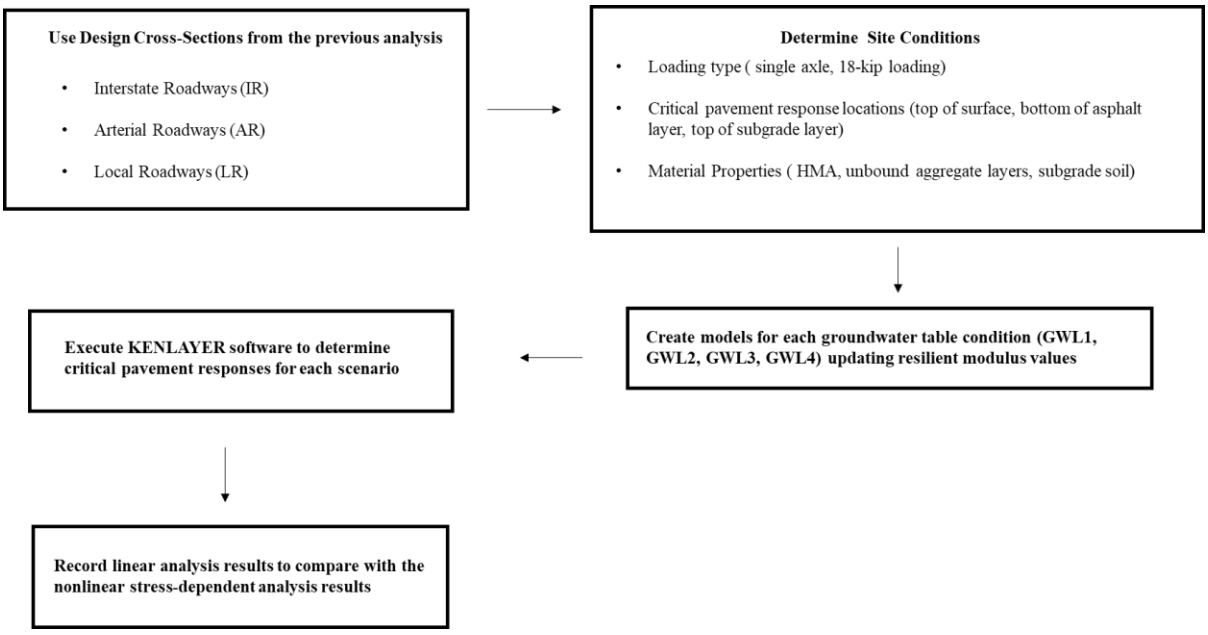

Figure 13 Linear Multi-layered Elastic Pavement Structural Analysis Flowchart

3.3.1.1 Pavement Structure Inputs

Table 13 summarizes the selected material inputs for KENLAYER linear multi-layered elastic analysis. The subgrade resilient modulus values were multiplied with the resilient modulus adjustment factors, which were 0.75 for the GWL2 condition and 0.5 for GWL3 and GWL4 conditions for the analysis.

Roadway Category	Layer Type	Resilient Modulus Input (psi) Groundwater Table Level			Thickness (inches)	Poisson's Ratio
		GWL1	GWL2	GWL3& GWL4		
Interstate Roads (IR)	Asphalt Concrete	450,000			7.5	0.35
	Limerock Base	24,000			11	0.40
	LBR40 Subbase	12,000			12	0.40
	Subgrade (Clayey Sand)	10,717	8,038	5,359	12	0.45
	Subgrade (Silty sand with gravel)	7,902	5,927	3,951	Semi-Infinite	0.45
Arterial Roads (AR)	Asphalt Concrete	450,000			4.5	0.35
	Limerock Base	24,000			10	0.40
	LBR40 Subbase	12,000			6	0.40
	Subgrade (Silty sand with gravel)	7,902	5,927	3,951	Semi-Infinite	0.45
Local Roads (LR)	Asphalt Concrete	450,000			2.5	0.35
	Limerock Base	24,000			8	0.35
	LBR40 Subbase	12,000			12	0.40
	Subgrade (Silty sand with gravel)	7,902	5,927	3,951	Semi-Infinite	0.45

Table 13: Pavement Structure Inputs for KENLAYER Linear-Elastic Pavement Analysis

3.3.2 Nonlinear Finite Element Solution-Based Pavement Analysis

Figure 14 depicts the pavement analysis flowchart using ABAQUS software to evaluate the impacts of stress-dependent nonlinear material behavior on Florida pavement structure performance.

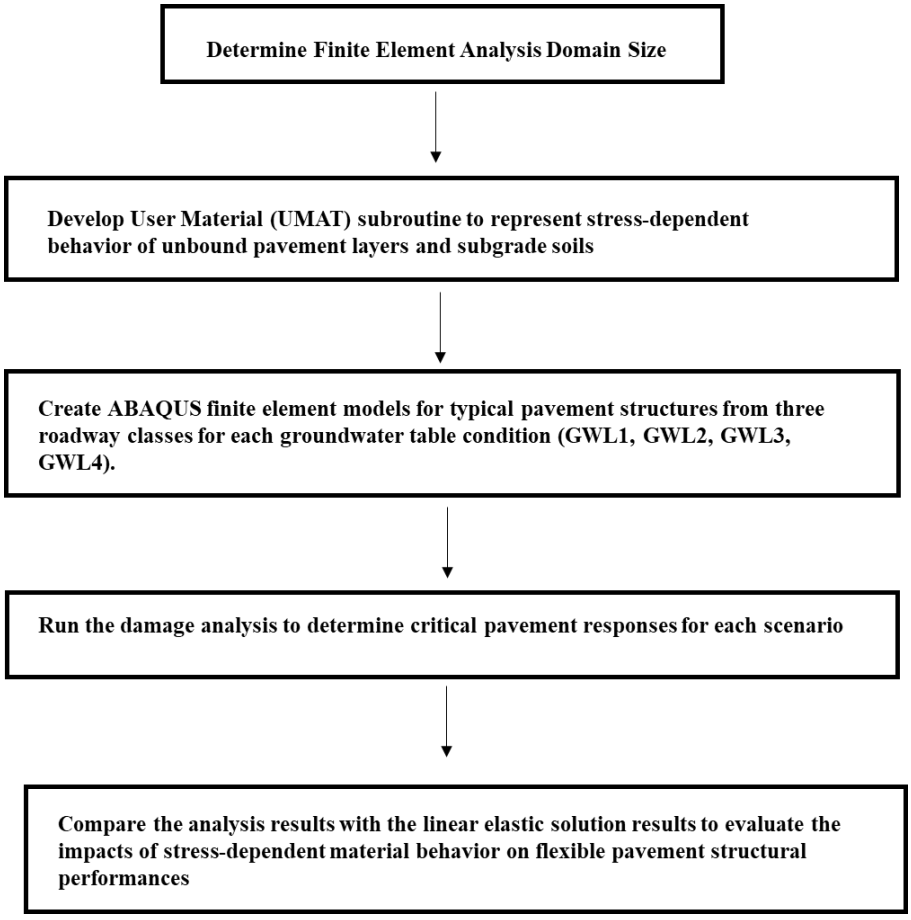

Figure 14: Nonlinear Finite Element Solution-based Pavement Structural Analysis Flowchart

3.3.2.1 Determining Finite Element Domain Size

ABAQUS software was used to investigate the impacts of material nonlinearity on the critical pavement responses. First of all, the most effective finite element domain size was determined as previously conducted studies showed that finite element model domain size affects the predicted responses and the accuracy of the finite element-based pavement analysis. In fact, Duncan et al. (53) obtained the most reasonable pavement analysis results when he selected the bottom fixed boundary depth as 50-times the radius

of the loading area (R) and the roller boundary at 12-times the radius of the loading area. Kim (38), on the other hand, found the domain size of 20-times the radius of the loading area from the center of loading in the horizontal distance and 140-times the radius of the loading area in the vertical direction as the most representative domain sizes for his study. The most representative domain size was determined for this study by conducting several linear elastic finite-element analyses with different domain sizes. Linear finite-element model analysis results, then, were compared with the KENLAYER software's linear analysis results.

The domain size of 20-times the radius of the loading area in the horizontal direction and 125-times the radius of the loading area in the vertical direction showed the closest results to the linear analysis solutions (Figure 15). The selected pavement cross-section for this analysis and the analysis results are depicted in Appendix C.

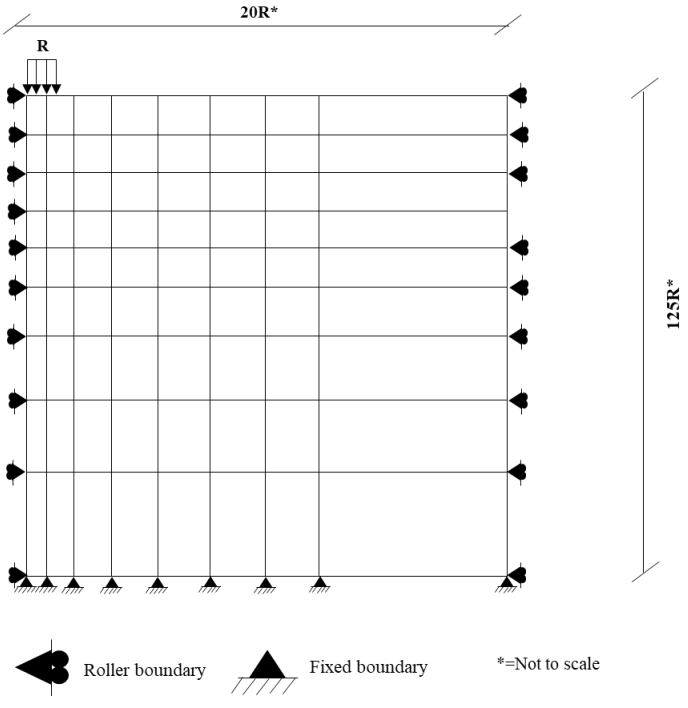

Figure 15: Selected Finite Element Domain Size and Boundaries for the Analysis

3.3.2.2 Developing a Nonlinear User-Defined Material Model

Programming a project-specific user-defined material (UMAT) subroutine code was required to characterize stress-dependent behavior of unbound pavement layers and subgrade soils. A direct secant stiffness solution technique proposed by Tutumluer (54) was adopted to generate the nonlinear solution by updating secant stiffness in each iteration. The nonlinear iteration schemes are performed using the stress-dependent models to calculate the actual resilient modulus corresponding to the stress level in every load increment.

General steps of the approach as described in Kim (38) and Gu (46) were followed for the purpose of this study. First of all, the necessary ABAQUS modeling inputs, a representative wheel load, the number of load increments, and convergence criteria were determined, along with the material properties and stress-dependent model constants. A wheel load was selected as 80 psi uniform pressure with 6 inches contact radius (R), and ten load increments were defined.

The ABAQUS model calculated the first stress state and incremental strain values by using the initial material properties. The secant resilient modulus values for each load increment were computed using Equation 8 at each integration point using the most recently calculated stresses in each element. The resilient modulus for the next iteration was obtained using the direct secant stiffness approach with the damping factor (λ) as shown in Equation 10 and then checked for convergence. A damping factor (λ) with values between 0 and 1 was adopted to avoid large material property and resilient modulus changes that could potentially create convergency problems.

$$M_R^{\,i} = (1-\lambda) \times M_R^{\,i-1} + \lambda \times M_{Rc}^{\,i}$$ Equation 10

where:

$M_R^{\,i}$ = actual resilient modulus value to be used at the end of iteration number(i)

$M_R^{\,i-1}$ = resilient modulus value used at previous iteration (i-1)

$M_{Rc}^{\,i}$ = computed resilient modulus from the model at the end of iteration number (i).

Two convergence criteria from the existing literature (38, 45, 46), the maximum individual error (E_i) and the maximum cumulative error (E_c), were utilized in this study, as shown in Equation 11 and Equation 12.

$$E_i = \frac{M_R^{\,i} - M_R^{\,i-1}}{M_R^{\,i}} \leq 5\%$$ Equation 11

$$E_c = \frac{\sum_{i=1}^{n} \left(M_R^{\,i} - M_R^{\,i-1} \right)^2}{\sum_{i=1}^{n} \left(M_R^{\,i} \right)^2} < 0.2\%$$ Equation 12

Figure 16 illustrates the flowchart of the developed UMAT subroutine for this analysis.

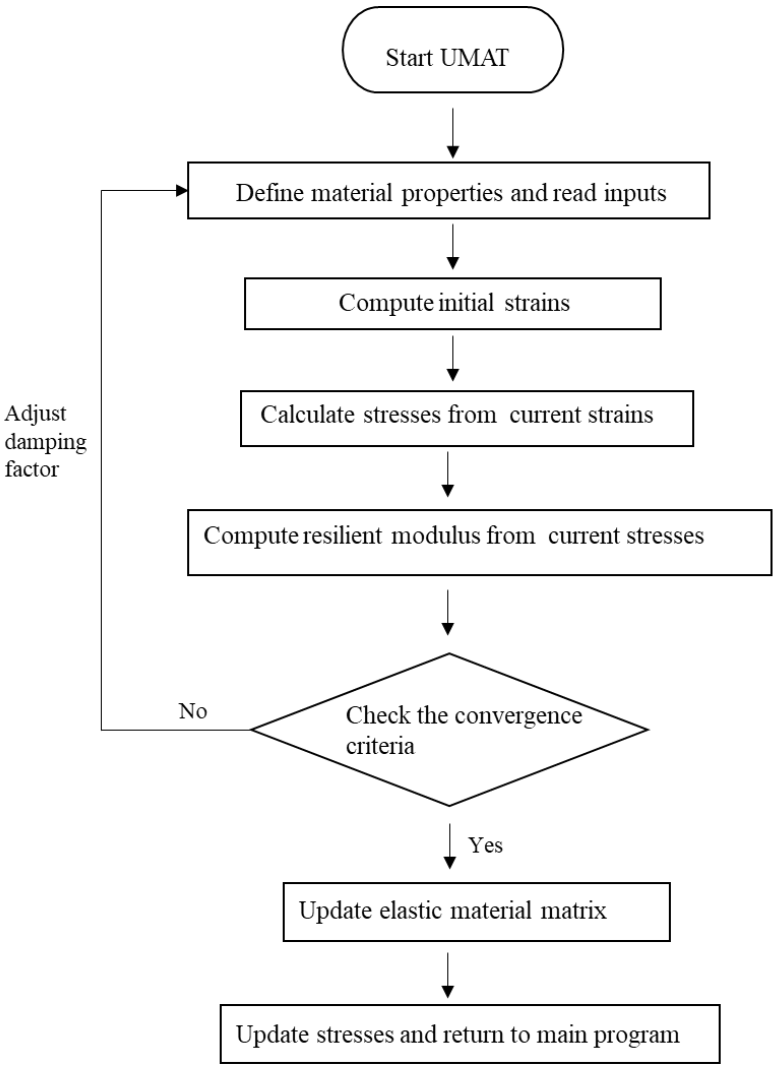

Figure 16: Flowchart of the Developed UMAT Subroutine

3.3.2.3 Pavement Structure Inputs

Table 14 summarizes the selected material inputs for ABAQUS nonlinear multi-layered elastic analysis.

Table 14: Pavement Structure Inputs for ABAQUS Nonlinear Pavement Analysis

Roadway Category	Layer Type	Element	Thickness (inches)	Poisson's Ratio	Initial Resilient Modulus Input (psi)		
					Groundwater Table Level		
					GWL1	GWL2	GWL3&GWL4
Interstate Roads (IR)	Asphalt Concrete	8-noded solid	7	0.35	450,000		
	Limerock Base	8-noded solid	11	0.40	24,000		
	LBR40 Subbase	8-noded solid	12	0.40	12,000		
	Subgrade (Clayey Sand)	8-noded solid	12	0.45	10,717	8,038	5,359
	Subgrade (Silty sand with gravel)	8-noded solid	708	0.45	7,902	5,927	3,951
Arterial Roads (AR)	Asphalt Concrete	8-noded solid	4.5	0.35	450,000		
	Limerock Base	8-noded solid	10	0.40	24,000		
	LBR40 Subbase	8-noded solid	12	0.40	12,000		
	Subgrade (Silty sand with gravel)	8-noded solid	723.5	0.45	7,902	5,927	3,951
Local Roads (LR)	Asphalt Concrete	8-noded solid	2.5	0.35	450,000		
	Limerock Base	8-noded solid	8	0.40	24,000		
	LBR40 Subbase	8-noded solid	12	0.40	12,000		
	Subgrade (Silty sand with gravel)	8-noded solid	727.5	0.45	7,902	5,927	3,951

Table 15 illustrates the stress-dependent model (Equation 9) constant values (k_1, k_2, k_3) for the base, subbase, and subgrade soils that were selected from the existing FHWA study (52) and the f_1 values that were adopted based on the FDOT flexible pavement design manual (32).

Table 15: Material Constants for ABAQUS Nonlinear Pavement Modeling

Layer Type	k_1	k_2	k_3	f_1		
				Groundwater Table Level Condition		
				GWL1	GWL2	GWL3&GWL4
Limerock Base	1131.11	0.68	-	1.00		
LBR40 Subbase	1000.85	0.53	-	1.00		
Subgrade (Clayey Sand)	834.87	0.35	-	1.00	0.75	0.50
Subgrade (Silty sand with gravel)	685.27	0.52	0.02	1.00	0.75	0.50

CHAPTER 4: RESULTS AND DISCUSSION

4.1 Empirical Pavement Structural Analysis Results

First of all, the AASHTO equation (Equation 1) was used to determine the allowable amount of traffic under optimum groundwater table condition (GWL1) for typical roadway sections and a comparison made with design traffic ESALS. Table 16 depicts the structural numbers and subgrade modulus inputs along with the predicted allowable traffic amount for each roadway classification.

Table 16: Empirical Analysis Results (Optimum Groundwater Condition)

Roadway Class	Design Structural Number (SN)	Subgrade Modulus (psi)	Allowable Traffic ESALS ($x10^6$)	Design Traffic ESALS ($x10^6$)
Interstate Roads (IR)	6.02	8,000	32.69	28.70
Arterial Roads (AR)	4.74	8,000	10.93	9.00
Local Roads (LR)	3.50	8,000	1.92	1.50

These results show that all roadway sections were designed to perform well at anticipated traffic levels. Next, the subgrade resilient modulus value within the AASHTO equation was reduced by 25% for 3.5’ groundwater table depth (GWT2) and by 50% for 2.5’ and 1.5’ groundwater table depth (GWT3 and GWT4) conditions.

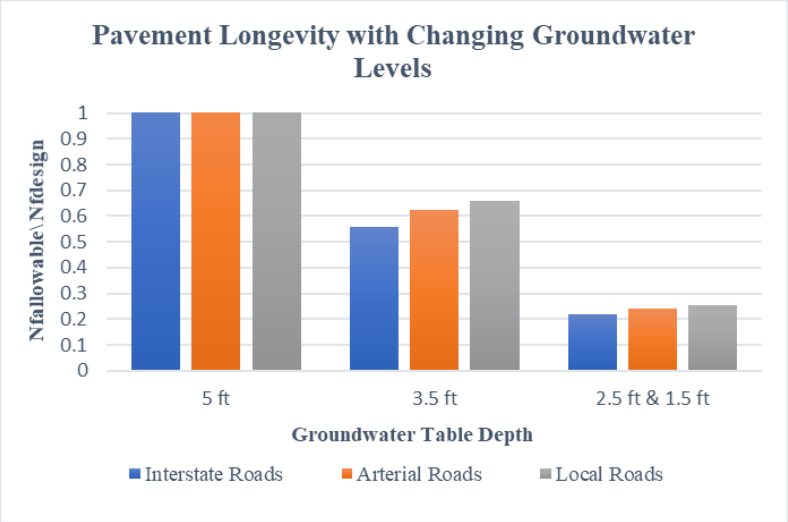

Figure 17: Empirical Analysis Results: Pavement Longevity with Rising Groundwater Level Conditions

Analysis results showed that the structural capacities of all roadway classes were reduced significantly when GWT depth was lower than 5 ft. Figure 17 shows the ratio between the allowable traffic ESALS under selected groundwater table conditions ($Nf_{allowable}$) to design traffic ESALS (Nf_{design}) for interstate, arterial and local roadway sections.

The pavement structural life reduction was considered when $\frac{Nf_{allowable}}{Nf_{design}} < 1$ and was calculated using Equation 16.

Pavement structural life reduction (in percent) = $1 - \frac{Nf_{allowable}}{Nf_{design}}$ Equation 16

The rising groundwater table levels impacted the typical interstate roadway the most and reduced its longevity by 42% when GWT depth is 3.5 ft and by 77% when GWT depth is 2.5 ft. Similarly, arterial roadway structural performance will be lowered by 38 percent if the GWT level reaches 3.5ft below the surface layer and 76% if only 2.5

ft GWT depth condition occurs. Typical local roadway section's longevity was the least impacted compared to typical arterial and interstate road sections. When GWT rose from 5 ft to 3.5 ft, local roadway longevity was reduced by 34%. The pavement section was predicted to face 74% longevity loss if GWT depth is 2.5 ft or lower from the surface level (Table 17).

Table 17: Predicted Pavement Longevity Loss using Empirical Analysis Method

Pavement Longevity Loss (%)			
Groundwater table depth	5 ft	3.5 ft	2.5 ft&1.5 ft
Interstate Roads (IR)	-	42%	77%
Arterial Roads (AR)	-	38%	76%
Local Roads (LR)	-	34%	74%

Since the FDOT manual (32) allows users to reduce resilient modulus input by up to 50%, resilient modulus inputs for two groundwater depth conditions (GWL3 and GWL4) were kept the same during the analysis. However, this assumption might fail to represent the magnitude of higher groundwater tables' (GWL4) impact on roadway sections or overpredict the lower groundwater tables' (GWL3) result. Another limitation of the empirical analysis was that the contributing distress type (fatigue cracking or rutting) for roadway failure could not be determined.

4.2 Mechanistic-Empirical (ME) Pavement Structural Performance Analysis Results

Pavement longevity with sea level rise-induced rising groundwater levels was predicted using the direct analysis outputs of the AASHTOWare software and compared with the optimum condition. In all pavement profiles, top-down fatigue cracking and asphalt only rutting were not influenced by any groundwater table level changes.

Terminal roughness (IRI) of pavement structures were only increased slightly but were not a cause of any predicted failure. On the other hand, the total rutting performance of pavement structures was significantly reduced when the GWT was not at the optimum (5 ft depth) condition. Alligator (bottom-up) fatigue cracking performance results showed variations for different roadway classes.

The longevity of the interstate roadway section was determined by alligator cracking when the average groundwater table depth is 5ft. The pavement was predicted to have structural cracking damage seventeen and half years after the road opening. Rising groundwater table levels reduce both rutting and alligator fatigue cracking the life expectancy of this section significantly. However, the pavement structure was predicted to face rutting failure earlier than the fatigue cracking. The IR's life expectancy was reduced by 42%, 52%, and 57% when GWL is 3.5 ft, 2.5 ft, and 1.5 ft., respectively (Figure 18).

Table 18: Interstate Roadway Damage Analysis Results

Distress Type	Distress @ Specified Reliability				
	Limit	Predicted (GWL1)	Predicted (GWL2)	Predicted (GWL3)	Predicted (GWL4)
Terminal IRI (in/mile)	172.00	159.54	161.6	162.63	163.25
Permanent deformation - total pavement (in)	0.40	**0.40**	**0.43**	**0.44**	**0.44**
AC bottom-up fatigue cracking (% lane area)	10.00	**16.43**	**21.46**	**24.14**	**25.76**
AC top-down fatigue cracking (% lane area)	20.00	6.01	6.01	6.01	6.01
Permanent deformation - AC only (in)	0.15	0.10	0.10	0.10	0.10

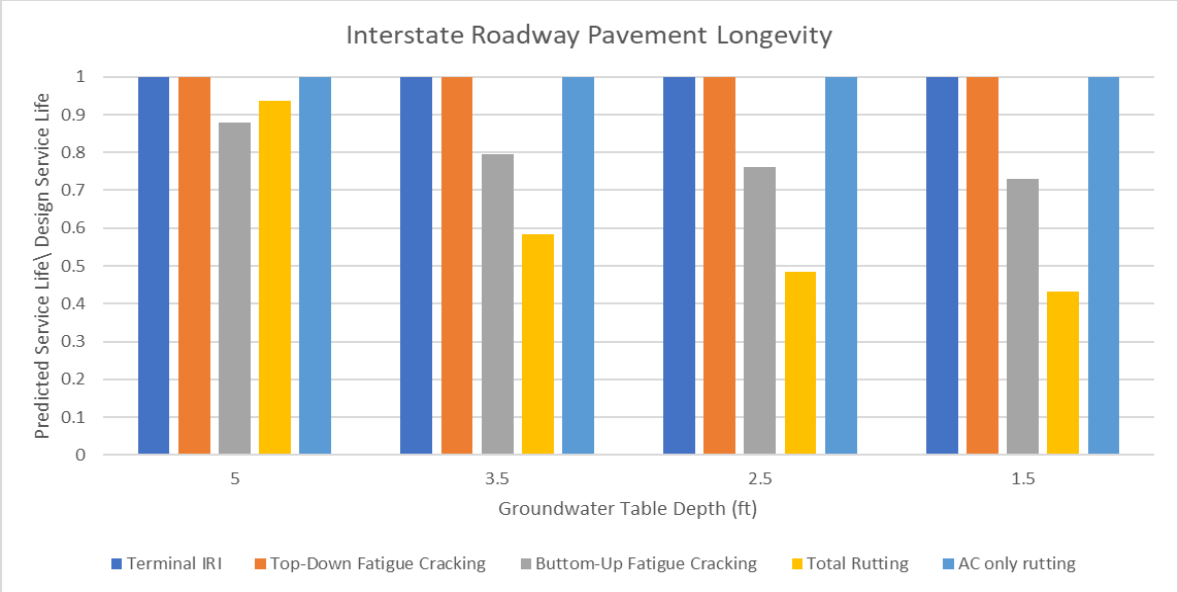

Figure 18: The Mechanistic-Empirical (ME) Analysis Interstate Roadway Section Pavement Longevity

The arterial roadway would not face excessive distress during the design service life under the optimum groundwater depth condition. The percentage of bottom-up fatigue cracking that occurs on the lane was projected to increase by up to 4 percent, but it would not cause a failure. Nevertheless, rising groundwater tables would increase the total rutting depth considerably. Thus, pavement longevity was determined by rutting performance and would be shortened dramatically. In the case of this section having 1.5 ft average GWT depth, pavement longevity would be shortened by 60% compared to design service life (Figure 19).

Table 19: Arterial Roadway Mechanistic-Empirical (ME) Damage Analysis Result

Distress Type	Distress @ Specified Reliability				
	Limit	Predicted (GWL1)	Predicted (GWL2)	Predicted (GWL3)	Predicted (GWL4)
Terminal IRI (in/mile)	172.00	150.06	151.77	152.64	153.60
Permanent deformation - total pavement (in)	0.50	0.50	**0.53**	**0.55**	**0.57**
AC bottom-up fatigue cracking (% lane area)	20.00	10.89	11.81	12.33	14.12
AC top-down fatigue cracking (% lane area)	20.00	3.76	3.76	3.76	3.76
Permanent deformation - AC only (in)	0.20	0.12	0.12	0.12	0.12

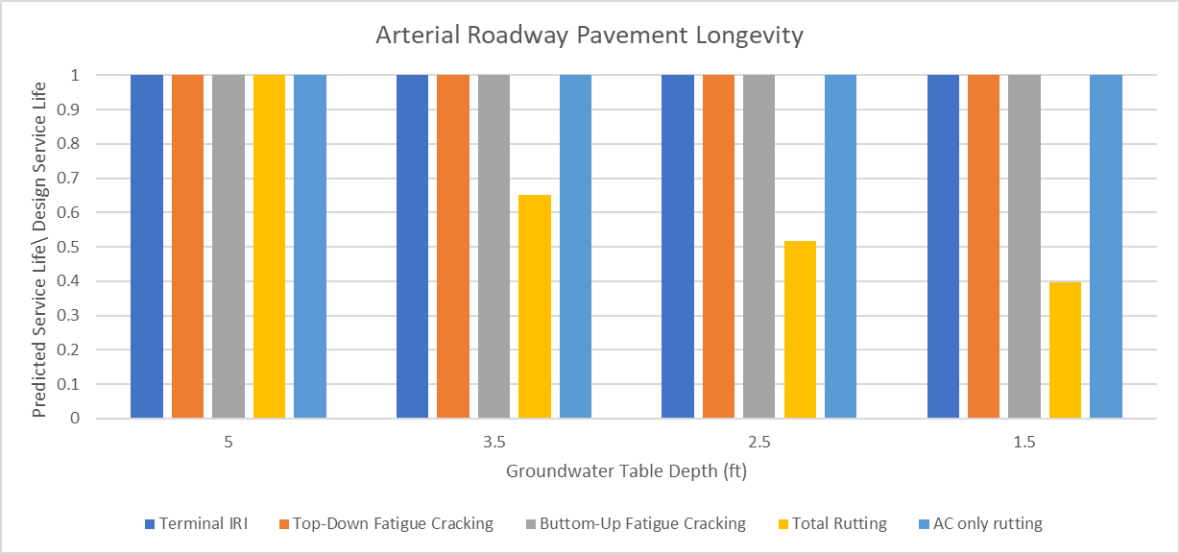

Figure 19: The Mechanistic-Empirical (ME) Analysis Arterial Roadway Section Pavement Longevity

The fatigue life of LR, unlike other roadway sections, would not see any changes even though this roadway profile has the thinnest asphalt layer. Under the optimum conditions, this pavement structure would serve 20 years without any failure. However, the rising groundwater table would increase the predicted total rutting depth for this pavement profile from 0.64 to up to 0.73 inches (Table 16). Therefore, the pavement structure would deteriorate much faster; the rutting distress would control the pavement longevity. The local roadways sections' life expectancy was lowered by 11%, 32%, and 52% when GWL is 3.5 ft, 2.5 ft, and 1.5 ft., respectively (Figure 20).

Table 20: Local Roadway Damage Analysis Result

Distress Type	Distress @ Specified Reliability				
	Limit	Predicted (GWL1)	Predicted (GWL2)	Predicted (GWL3)	Predicted (GWL4)
Terminal IRI (in/mile)	172.00	150.48	151.58	152.86	153.60
Permanent deformation - total pavement (in)	0.65	0.64	**0.67**	**0.69**	**0.73**
AC bottom-up fatigue cracking (% lane area)	35.00	0.97	0.97	0.98	1.00
AC top-down fatigue cracking (% lane area)	35.00	3.08	3.08	3.08	3.08
Permanent deformation - AC only (in)	0.30	0.12	0.12	0.12	0.12

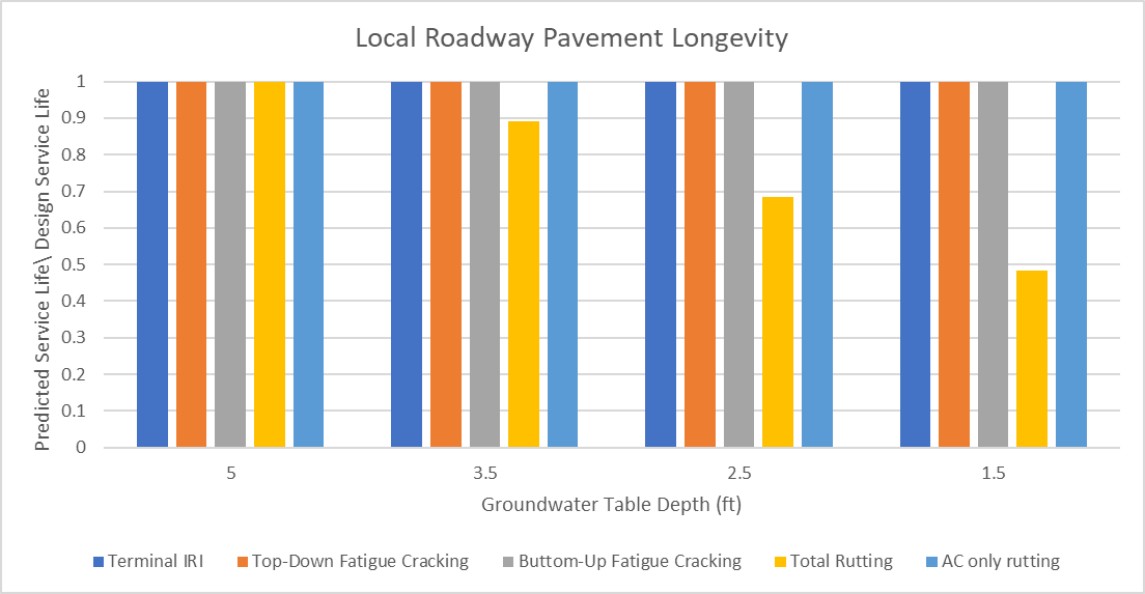

Figure 20: The Mechanistic-Empirical (ME) Analysis Local Roadway Section Pavement Longevity

In conclusion, typical arterial and local roadway sections were designed to perform adequately under optimum groundwater table conditions. However, the interstate roadway was predicted to face fatigue cracking failure after serving 17.5 years. Rising groundwater table levels lowered the life expectancy of all roadway classes. All roadway classes were expected to face rutting failure when the GWT level reached 3.5 ft below the surface level or higher. A typical interstate roadway section faced the highest rates of

structural life reductions when the GWT level was 5, 3.5, and 2.5 ft below the surface (Figure 21).

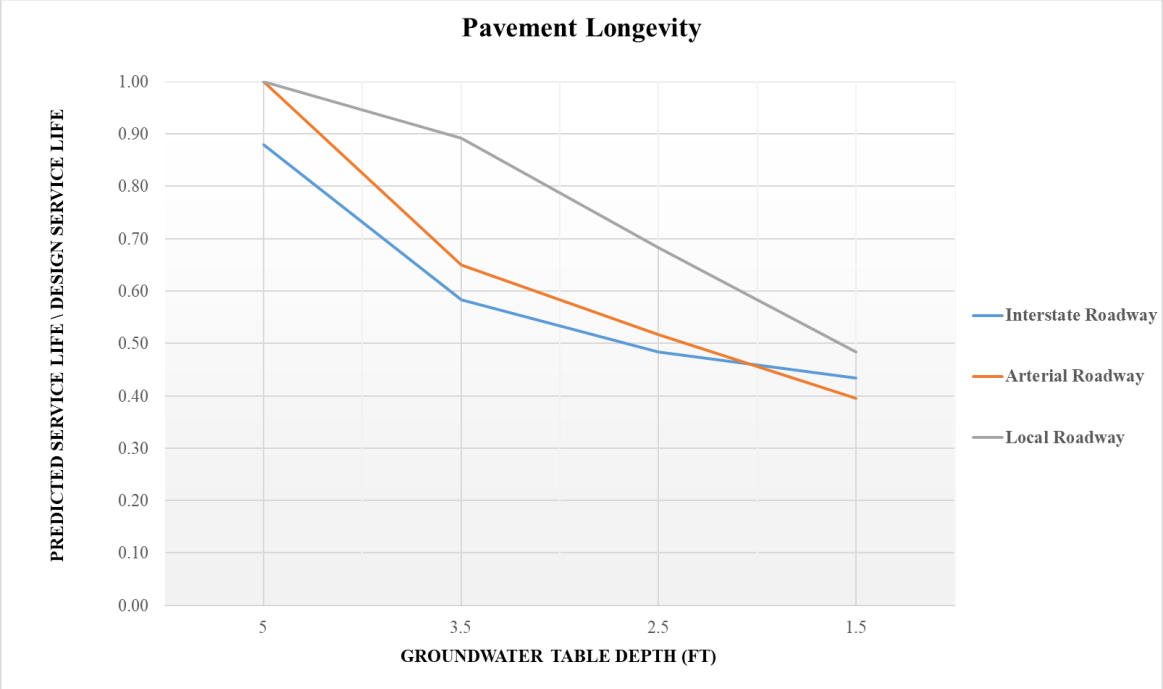

Figure 21: The Mechanistic-Empirical (ME) Damage Analysis Results: Predicted Pavement Longevity for Three Roadway Classes

On the other hand, having higher performance criteria and lower reliability levels played a positive role in the higher life expectancy of the typical local roadway class than the other two functional classes. For example, Figure 22 depicts the predicted rutting depth (inches) for interstate, arterial, and local roadway structures under four groundwater table depth conditions. Although local roadway was expected to face the highest rutting depth (0.64 inches) under the optimum groundwater table condition (GWL1), it was predicted to have 20-year service life because the predicted rutting depth was lower than the limit (0.65 inches) for this roadway section. On the contrary, the

interstate roadway was limited to have a maximum of 0.40 inches rutting. The ME analysis output predicted 0.401 inches of rutting depth after 17.5 years of service. Thus, IR was expected to have the lowest longevity compared to other roadway structures.

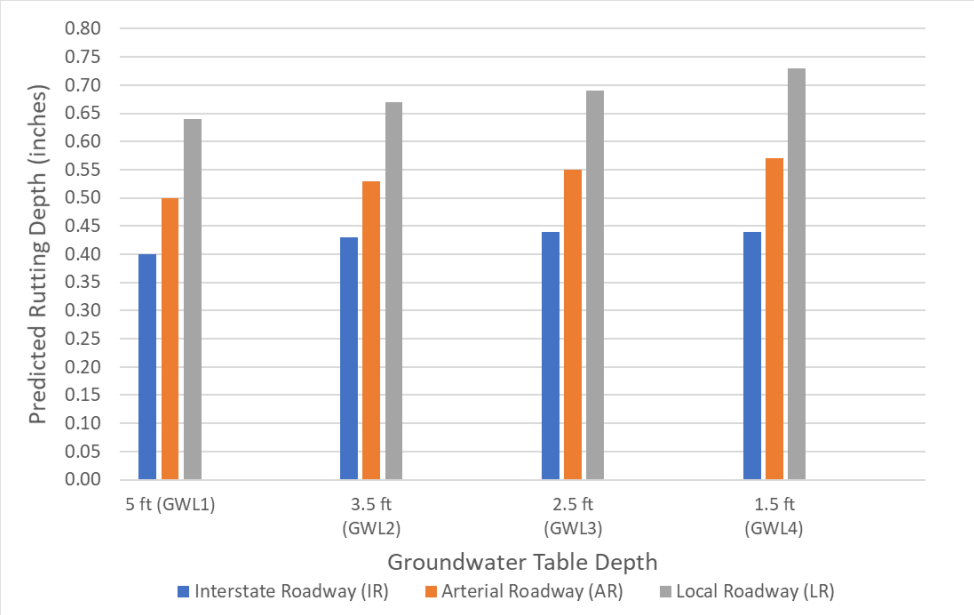

Figure 22: Predicted Rutting Depth (inches) for Interstate, Arterial, and Local Roadway Structures Under Four Groundwater Table Depth Conditions

It should be noted that there have not been any local calibration studies in Florida to be used in AASHTOWare software. Therefore, nationally calibrated empirical models within the AASHTOWare software were used in this study.

4.3 Comparison of Empirical Analysis Results with Mechanistic-Empirical (ME) Analysis Results

Table 21 summarizes the pavement longevity losses that were predicted from both empirical and AASHTOWare software analysis and selected groundwater table depth conditions. Overall, both analysis approaches expected a significant level of structural

capacity losses for all roadway classes. The empirical approach mostly predicted higher longevity losses compared to AASHTOWare software results. The only exception occurred when AASHTOWare software forecasted a failure on the typical interstate roadway section when GWT depth was 5 ft below the surface (Table 21).

Table 21: Comparison of Empirical and The Mechanistic-Empirical (ME) Damage Analysis Results

Pavement Longevity Loss							
Analysis Method	Empirical Damage Analysis			AASHTOWare ME Damage Analysis			
Groundwater table depth	5 ft	3.5 ft	2.5 ft&1.5 ft	5 ft	3.5 ft	2.5 ft	1.5 ft
Interstate Roads (IR)	-	42%	77%	12%	42%	52%	57%
Arterial Roads (AR)	-	38%	76%	-	35%	48%	60%
Local Roads (LR)	-	34%	74%	-	11%	32%	52%

Empirical damage analysis results predicted interstate roadways to be the most vulnerable roadway for rising groundwater table levels problems. AASHTOWare software agreed with this prediction except when GWT is 1.5 ft below the surface level. The arterial roadway was predicted to lose 60% of its structural capacity under this condition. Conversely, both analyses indicated the lowest pavement longevity loss for the typical local roadway section based on the selected performance criteria and reliability levels.

Moreover, the empirical analysis was unable to determine different pavement longevity losses for 2.5 ft and 1.5 ft groundwater table conditions because the FDOT flexible pavement design manual (32) uses the same adjustment factor (0.5) for both conditions. Finally, AASHTOWare was able to determine the contributing distress that would cause the pavement failure.

4.4 Evaluation of the Impacts of Material Nonlinearity on Critical Pavement Responses

ABAQUS and KENLAYER software were used to investigate the influence of material stress-dependent nonlinearity on critical pavement responses in Florida. The Stress-dependent material model was programmed using the UMAT function of ABAQUS software. Therefore, the actual resilient modulus values of each element were calculated from the stress state. Figures 23, 24, and 25 depict the contours of predicted resilient modulus by ABAQUS software for the arterial roadway section's base, subbase, and subgrade layers, respectively. Due to the stress-hardening material behavior, the higher resilient modulus values were observed under the centerline of the loading. By applying the nonlinear material model, the variances created in horizontal and vertical directions of each layer were considered for the structural pavement analysis.

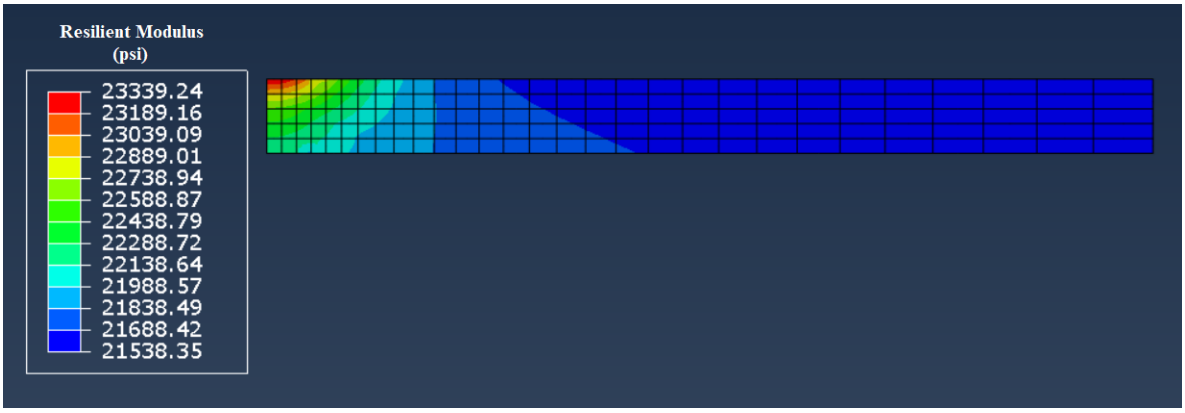

Figure 23: Contour of Predicted Resilient Modulus by ABAQUS Software for the Base Layer

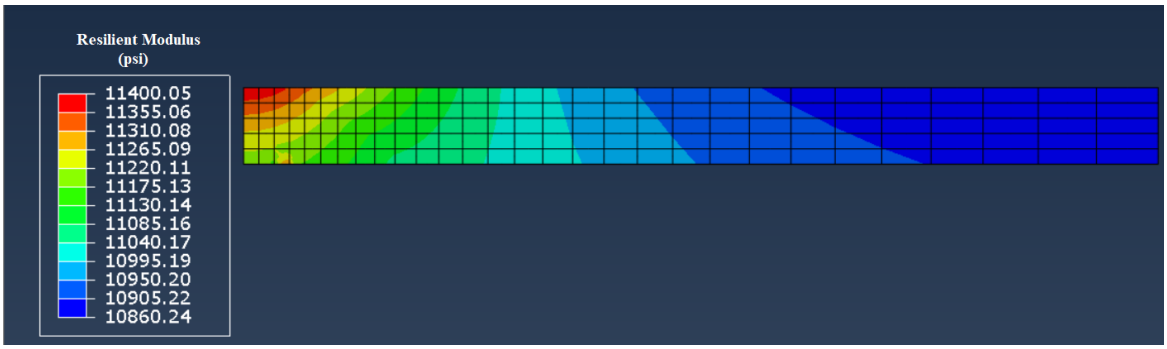

Figure 24: Contour of Predicted Resilient Modulus by ABAQUS Software for the Subbase Layer

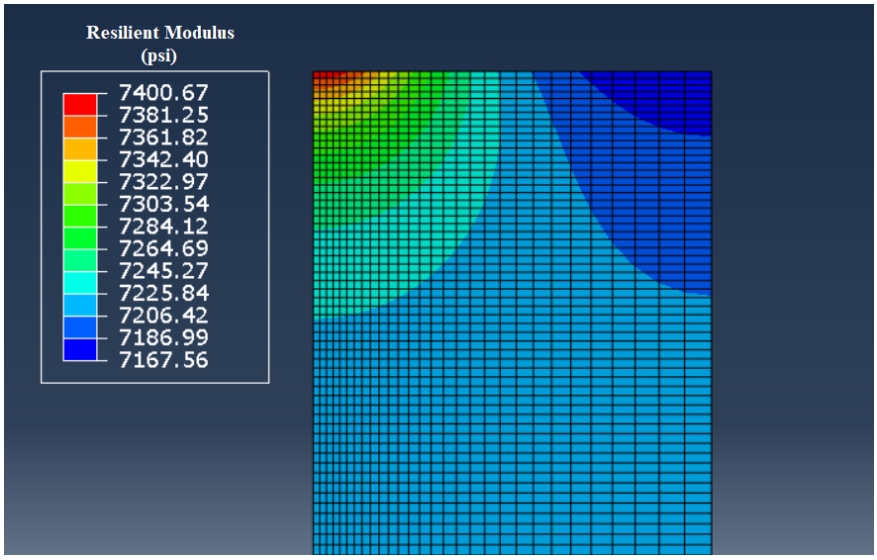

Figure 25: Contour of Predicted Resilient Modulus by ABAQUS Software for the Subgrade Layer

The critical pavement responses, which are vertical deflection on the asphalt layer surface, horizontal tensile strain at the bottom of the asphalt layer, and vertical compressive strain on the top of the subgrade layer, were predicted when they were subjected to a wheel load. Figure 26 compares the predicted horizontal tensile strain at the bottom of the asphalt layer from linear and nonlinear analysis for selected groundwater table depth scenarios.

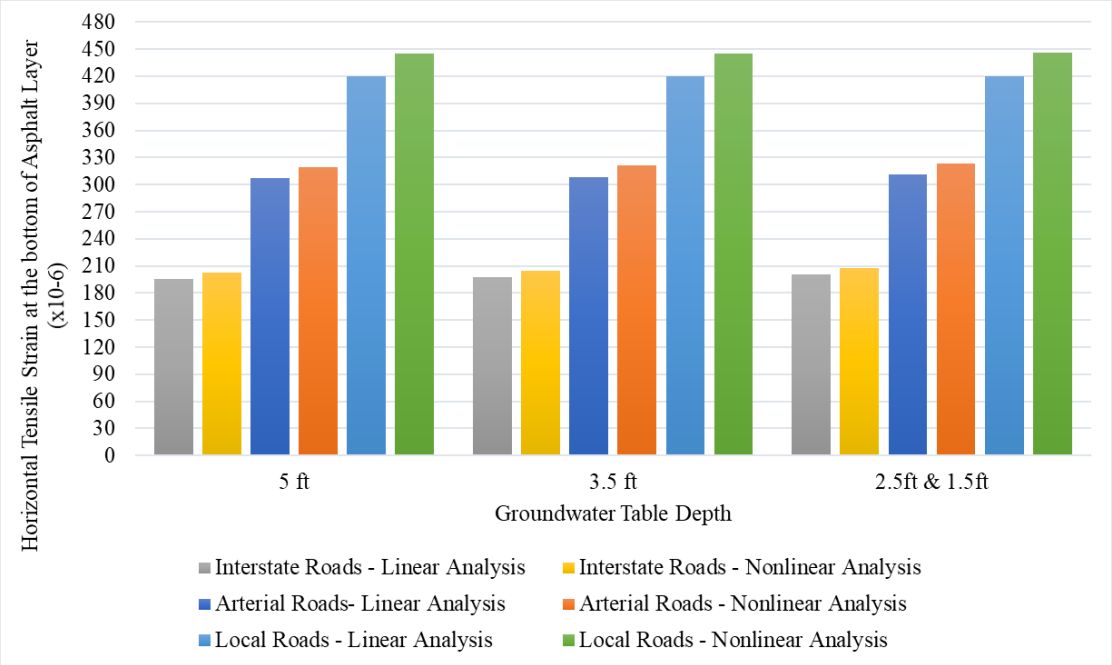

Figure 26: Comparison of Tensile Strain at the Bottom of Asphalt Layer Between Linear and Nonlinear Analysis for Three Roadway Classes

It was seen that material stress-dependent nonlinear behavior increases the tensile strain by 4% for the interstate roadway section and arterial section and by 6% for the local roadway section in each groundwater table condition. The fatigue life of the flexible pavement is linked with the predicted tensile strains at the bottom of the asphalt layer and cannot be drastically affected by stress-dependent nonlinear behavior.

The vertical tensile strain at the top of the subgrade layer is linked with the rutting life of pavement structures. Figure 27 compares the linear and nonlinear analysis predictions for the selected groundwater table depth scenarios. It was observed that nonlinear material behavior increased the vertical strain at the top of the subgrade layer by 2 to 3% for the arterial and local roadway structures. On the other hand, a 2% increase was noted for the typical interstate roadway structure. Thus, the rutting life expectancy of

the selected pavement structures will not be impacted dramatically by stress-dependent material nonlinearity.

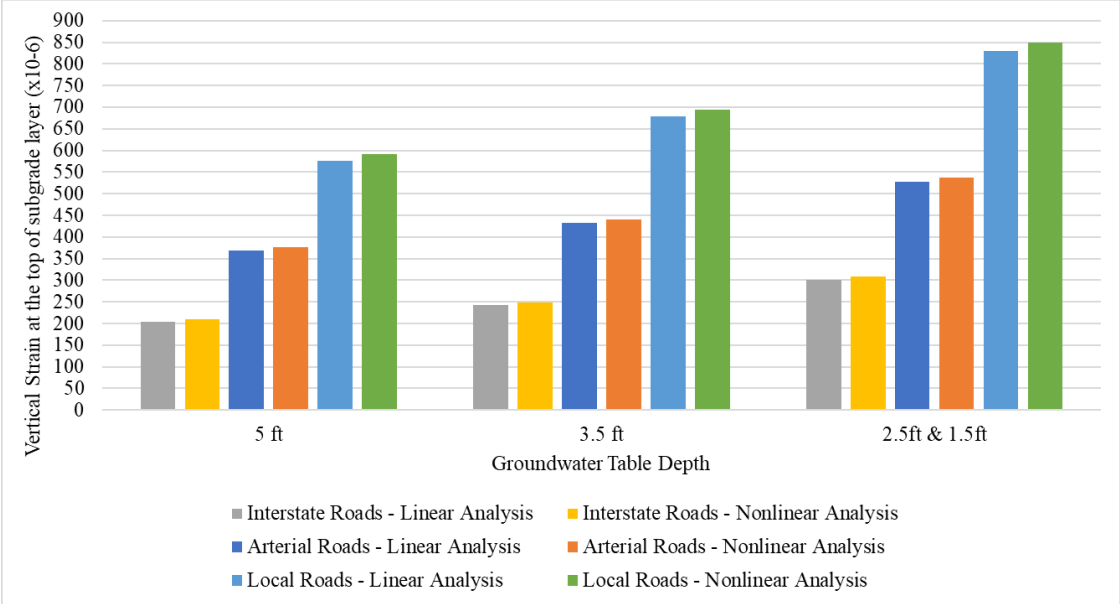

Figure 27: Comparison of Vertical Strain at the Top of Subgrade Layer Between Linear and Nonlinear Analysis for Three Roadway Classes

Figure 28 depicts the surface deflection predictions from linear and nonlinear analysis for each roadway class. Stress-dependent soil nonlinearity consistently increased the predicted surface deflection, however, in small percentages. A 5 % increase was observed for the interstate roadway section, while up to a 4% increase was noted for the typical arterial and local pavement structures.

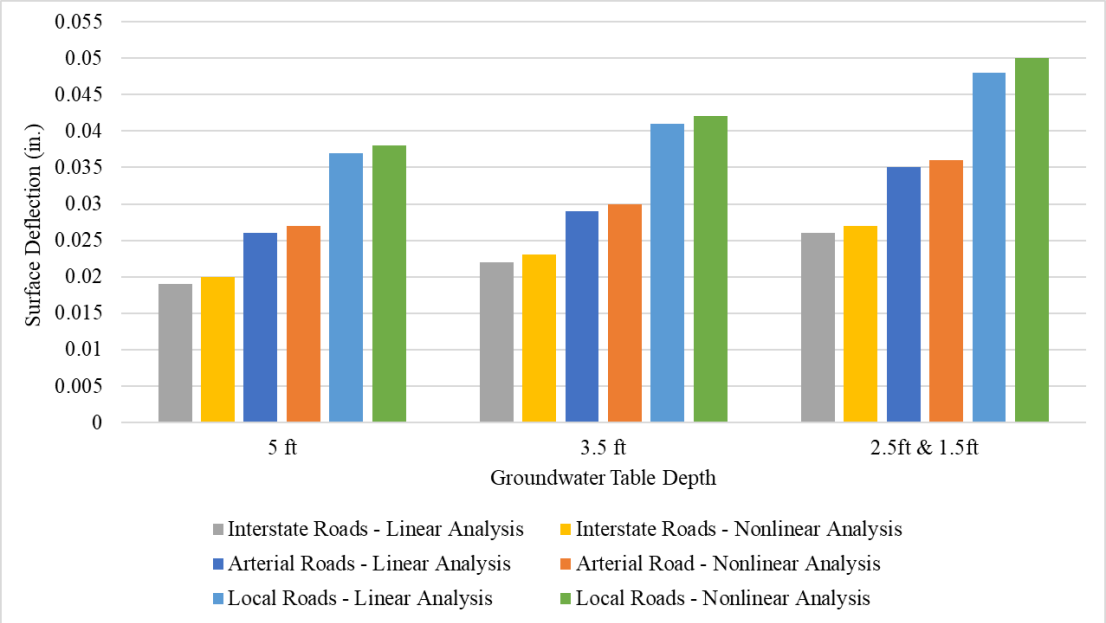

Figure 28: Comparison of Surface Deflection Between Linear and Nonlinear Analysis for Three Roadway Classes

CHAPTER 5: CONCLUSION, LIMITATIONS, AND RECOMMENDATIONS

5.1 Conclusion

Rising sea levels threaten US coastal counties by elevating the groundwater table. Subjecting roadways with a potentially weakened structural capacity to traffic loading can result in premature distress, structural failure, and reduced service life. Therefore, this thesis investigated the potential effects of sea-level rise-induced high groundwater table levels on typical Florida flexible pavement structural performance.

Within the limitation of the model and computation herein used, the four research objectives were met as shown below:

1. The longevity of typical Florida flexible pavement structures with rising groundwater table conditions was determined by conducting empirical and mechanistic-empirical (ME) pavement damage analyses. The analysis results showed that sea-level rise-induced high groundwater table significantly reduced the service life of typical Florida pavement sections. All selected roadway classifications (IR, AR, LR) were projected to face pavement failure within their design life when GWT is 3.5 ft or higher.
2. The effects of rising groundwater table (GWT) levels in Florida on pavement performance parameters (roughness, fatigue cracking, and rutting) were assessed. The causes of pavement failures under different GWT conditions were determined. The empirical analysis did not predict any failures when GWT was optimum 5 ft depth condition. However, the mechanistic-empirical analysis predicted a fatigue failure for the selected interstate pavement

structure when GWT depth was 5 ft. The output of mechanistic-empirical analysis also indicated that rising groundwater table levels in Florida would affect the rutting performance more considerably than the predicted fatigue cracking and roughness performance of the selected roadway structures. Thus, all pavement structures (interstate, arterial and local roadway) were expected to face rutting failure when the GWT level was 3.5 ft, 2.5 ft, and 1.5 ft below the surface level.

3. The analysis results from the existing empirical approach and the mechanistic-empirical (ME) approach were compared. The AASHTO'93 empirical approach and AASHTOWare ME software predicted the roadway sections' longevity loss in a consistent manner; although, empirical analysis results usually projected higher magnitudes of service life reductions.
4. The influence of nonlinear stress-dependent material behavior on critical pavement responses was evaluated by comparing linear elastic pavement analysis with finite element method-based nonlinear analysis. Stress-dependent nonlinear material behavior increased the predicted surface deflection and the predicted tensile strain at the bottom of the asphalt layer by 4 to 6%. In addition, nonlinear material behavior increased the predicted vertical strain at the top of the subgrade layer by 2 to 3% for the arterial and local roadway structures. On the other hand, a 2% decrease was noted for the typical interstate roadway structure. Therefore, the nonlinear material behavior was found to have minor effects (2% to 6%) on Florida flexible pavement structural performance.

5.2 Limitations

This study did not consider flooded conditions when the sea-level rise is coupled with storm surge or intense rainstorms. Such actions are likely to create more challenging conditions and more accelerated damage.

The groundwater table levels were selected as an average depth, and yearly groundwater fluctuations during the pavement design life were not considered due to the AASHTOWare modeling limitations.

The nationally calibrated AASHTOWare software models were used for the damage analysis as there has not been any local calibration study in Florida. The predicted pavement longevity loss under selected groundwater table conditions could alter when these studies are completed.

The limited amount of soil types and material properties which were available in the literature were investigated for the stress-dependent analysis.

5.3 Recommendations

This study conducted damage analysis for Florida's flexible pavement structure by using both the current practice in Florida and the state-of-practice computer software to predict potential pavement service life changes in case of rising groundwater tables. It is recommended that the local agencies consider the expected rates of structural life loss for the roadway sections under different groundwater table rise scenarios. Additionally, the rutting performance of roadway sections was reduced significantly due to having high groundwater table levels so that it would control the design life of the structures.

Therefore, local agencies can plan their maintenance budgeting and potential adaptation strategies accordingly to prevent rutting failure for their highways in the future.

The future effort for this study should include the field measurements and observations of the pavement structures experiencing different groundwater table levels to address the key limitations of this study. Developing a test pit would allow researchers to simulate the yearly groundwater fluctuations and couple the flooding condition with rising groundwater table levels to conduct a more comprehensive study.

In addition, future studies that consider not only the stress-dependent but also moisture-dependent nonlinear characteristics of base, subbase, and subgrade soils could identify more significant changes in the flexible pavement structural performances. Therefore, developing more comprehensive finite element models to simulate the Florida flexible pavement structural behavior is also recommended.

REFERENCES

[1] National Research Council, Committee on Climate Change, US Transportation, Transportation Research Board, Division on Earth, & Life Studies. (2008). Potential impacts of climate change on US transportation: Special report 290 (Vol. 290). Transportation Research Board.

[2] Meyer, M. D., & Weigel, B. (2011). Climate change and transportation engineering: Preparing for a sustainable future. Journal of Transportation Engineering, 137(6), 393-403.

[3] IPCC, 2019: Technical Summary [H.-O. Pörtner, D.C. Roberts, V. Masson-Delmotte, P. Zhai, E. Poloczanska, K. Mintenbeck, M. Tignor, A. Alegría, M. Nicolai, A. Okem, J. Petzold, B. Rama, N.M. Weyer (eds.)]. In: IPCC Special Report on the Ocean and Cryosphere in a Changing Climate [H.- O. Pörtner, D.C. Roberts, V. Masson-Delmotte, P. Zhai, M. Tignor, E. Poloczanska, K. Mintenbeck, A. Alegría, M. Nicolai, A. Okem, J. Petzold, B. Rama, N.M. Weyer (eds.)]. In press

[4] Sweet, W. V., Kopp, R. E., Weaver, C. P., Obeysekera, J., Horton, R. M., Thieler, E. R., & Zervas, C. (2017). GLOBAL AND REGIONAL SEA LEVEL RISE SCENARIOS FOR THE UNITED STATES. NOAA Technical Report NOS CO-OPS 083. January, 75. https://tidesandcurrents.noaa.gov/publications/techrpt83_Global_and_Regional_SLR_Scenarios_for_the_US_final.pdf

[5] Vitousek, S., Barnard, P. L., Fletcher, C. H., Frazer, N., Erikson, L., & Storlazzi, C. D. (2017). Doubling of coastal flooding frequency within decades due to sea-level rise. Scientific reports, 7(1), 1-9.

[6] NOAA Office for Coastal Management (2021). Fast Facts: Florida. Retrieved from https://coast.noaa.gov/states/florida.html

[7] Knott, J. F., Jacobs, J. M., Daniel, J. S., & Kirshen, P. (2019). Modeling Groundwater Rise Caused by Sea-Level Rise in Coastal New Hampshire. Journal of Coastal Research, 35(1), 143–157. https://doi.org/10.2112/JCOASTRES-D-17-00153.1

[8] Masterson, J. P., M. N. Fienen, E. R. Thieler, D. B. Gesch, B. T. Gutierrez, and N. G. Plant (2014). Effects of Sea-Level Rise on Barrier Island Groundwater System Dynamics – Ecohydrological Implications. Ecohydrology, Vol. 7, No. 3, 2014, pp. 1064-1071. https://dx.doi.org/10.1002/eco.1442

[9] Walter, D. A., Mccobb, T. D., Masterson, J. P., & Fienen, M. J. (2016). Potential Effects of Sea-Level Rise on the Depth to Saturated Sediments of the Sagamore and Monomoy Flow Lenses on Cape Cod, Massachusetts. US Geological Survey Scientific Investigations Report 2016–5058, October, 55. https://pubs.er.usgs.gov/publication/sir20165058

[10] Knott, J. F., Daniel, J. S., Jacobs, J. M., and Kirshen, P. (2018). Adaptation Planning to Mitigate Coastal-Road Pavement Damage from Groundwater Rise Caused by Sea-Level Rise. Transportation Research Record: Journal of the Transportation Board, 2018. 2672(2): 11-22.

[11] Patel, V. J., Kumavat, H., Tapkire, G., Patil, D.R. (2016). Road Pavement Design for Heavy Ground Water Table in Shirpur and Surrounding Area. International Journal of Civil Engineering and Technology(IJCIET): Volume 7, Issue 1, Jan-Feb 2016, pp. 416-426, Article ID: IDCIET_07_01_031, http://www.iaeme.com/IJCIET/issues.asp?JType=IJCIET&VType=1

[12] IPWEA (2001). Local government salinity management handbook- A resource guide for the public works professional, Institute of Public Works Engineering Australia: Sydney NSW.

[13] Roshani, A. (2014). Road Infrastructure Vulnerability to Groundwater Table Variation due to Sea Level Rise. MS thesis. Queensland University of Technology, Australia, 2014.

[14] Knott, J. F., J. S. Daniel, J. M. Jacobs, P. Kirshen, and M. Elshaer (2017). Assessing the Effects of Rising Groundwater from Sea-Level Rise on the Service Life of Pavements in Coastal Road Infrastructure. Transportation Research Record: Journal of Transportation Research Board, 2017. 2639: 1–10.

[15] Shi-Jin Feng, Yi-Cheng Li, H. X. Chen & Zhang-Long Chen (2017). Response of pavement and stratified ground due to vehicle loads considering the rise of the water table, International Journal of Pavement Engineering, DOI: 10.1080/10298436.2017.1279486

[16] AASHTO (2015). Mechanistic-Empirical Pavement Design Guide: A Manual of Practice. Washington, DC: American Association of State Highway and Transportation Officials (AASHTO).

[17] AASHTO (1993). AASHTO Guide for Design of Pavement Structures. Washington, DC: American Association of State Highway and Transportation Officials (AASHTO).

[18] Beriha, B., Sahoo, U. C., & Mishra, D. (2020). Crosspave: a multi-layer elastic analysis programme considering stress-dependent and cross-anisotropic behaviour of unbound aggregate pavement layers. International Journal of Pavement Engineering, 1-15.

[19] European Environment Agency (2020). Data and Maps: Global and European Sea Level Rise. https://www.eea.europa.eu/data-and-maps/indicators/sea-level-rise-7/assessment

[20] Dangendorf, S., Hay, C., Calafat, F. M., Marcos, M., Piecuch, C. G., Berk, K., & Jensen, J. (2019). Persistent acceleration in global sea-level rise since the 1960s. Nature Climate Change, 9(9), 705-710.

[21] Raimi, D., Keyes, A., & Kingdon, C. (2020). Florida Climate Outlook. Resources for the Future, 20(01), 1–67. https://media.rff.org/documents/Florida_Climate_Outlook.pdf

[22] NOAA (2020). Relative Sea Level Trend, 8724580 8723214 Virginia Key, Florida. https://tidesandcurrents.noaa.gov/sltrends/sltrends_station.shtml?id=8723214

[23] Southeast Florida Regional Climate Change Compact Sea Level Rise Work Group (Compact). February 2020. A document prepared for the Southeast Florida Regional Climate Change Compact Climate Leadership Committee. 36p. https://southeastfloridaclimatecompact.org/wp-content/uploads/2020/04/Sea-Level-Rise-Projection-Guidance-Report_FINAL_02212020.pdf

[24] Befus, K. M., Barnard, P. L., Hoover, D. J., Finzi Hart, J. A., & Voss, C. I. (2020). The increasing threat of coastal groundwater hazards from sea-level rise in California. Nature Climate Change, 10(10), 946–952. https://doi.org/10.1038/s41558-020-0874-1

[25] Werner, A. D., & Simmons, C. T. (2009). Impact of sea-level rise on seawater intrusion in coastal aquifers. Ground Water, 47(2), 197-204.

[26] Rotzoll, K., & Fletcher, C. H. (2013). Assessment of groundwater inundation as a consequence of sea-level rise. Nature Climate Change, 3(5), 477-481.

[27] Roshani, A., Gallage, C. (2013): Groundwater Table response to Sea Level Rise and its Impact on Pavement Structure. Conference Paper in the conference: 9th Annual International Conference of the International Institute for Infrastructure Renewal and Reconstruction, At Queensland University of Technology, Brisbane, Australia

[28] Decker, J.D., Hughes, J.D., and Swain, E. D. (2018). Potential for Increased Inundation in Flood-Prone Regions of Southeast Florida in Response to Climate and Sea-Level Changes in Broward County, Florida, 2060–69.

[29] Sukop, M. C., Rogers, M., Guannel, G., Infanti, J. M., & Hagemann, K. (2018). High temporal resolution modeling of the impact of rain, tides, and sea-level rise on water table flooding in the Arch Creek Basin, Miami-Dade County, Florida USA. Science of the Total Environment, 616–617, 1668–1688. https://doi.org/10.1016/j.scitotenv.2017.10.170

[30] Obeysekera, J., Sukop, M., Tiffany, T., Irizarry, M., & Rogers, M. (2019). Potential Implications of Sea-Level Rise and Changing Rainfall for Communities in Florida using Miami-Dade County as a Case Study. Miami FL: Sea Level Solutions Center, Florida International University. Retrieved from https://slsc.fiu.edu/_assets/pdfs/fbc_fiu_finalreport_22aug2019.pdf

[31] Rojali, A., Gocmez, M. G., Ali, H. A., & Fuentes, H. R. (2021). Improvement and Benefit of Updated Vulnerability Maps of Pavement Infrastructure Affected by Sea-Level Rise: A Case in South Florida. Asia Oceanic Geosciences Society: 18th Annual Meeting.

[32] Florida Department of Transportation (2021). Florida Flexible Pavement Design Manual. Retrieved from: https://fdotwww.blob.core.windows.net/sitefinity/docs/default-source/roadway/pm/publications/2021-fpdm-final.pdf?

[33] Jonathan Boone (2013). Comparison of Ontario Pavement Designs Using the AASHTO 1993 Empirical Method and the Mechanistic-Empirical Pavement Design Guide Method. UWSpace http://hdl.handle.net/10012/8047

[34] Ping, W. V., & Ling, C. C. (2008). Design Highwater Clearances for Highway Pavements. Volume I (No. FL/DOT/RMC/BD-543-13).

[35] Carvalho, R. L., & Schwartz, C. W. (2006). Comparisons of flexible pavement designs: AASHTO empirical versus NCHRP project 1–37A mechanistic-empirical. Transportation Research Record, 1947(1), 167-174.

[36] Fredlund, D. G., & Xing, A. (1994). Equations for the soil-water characteristic curve. Canadian geotechnical journal, 31(4), 521-532.

[37] Witczak, M. W., Zapata, C. E., & Houston, W. N. (2006). Models incorporated into the current enhanced integrated climatic model: NCHRP 9-23 project findings and additional changes after version 0.7. Final Report, Project NCHRP.

[38] Kim, M. (2007). Three-dimensional finite element analysis of flexible pavements considering nonlinear pavement foundation behavior. The University of Illinois at Urbana-Champaign.

[39] Rada, G. R., Nazarian, S., Visintine, B. A., Siddharthan, R. V., & Thyagarajan, S. (2016). Pavement structural evaluation at the network level (No. FHWA-HRT-15-074). The United States. Federal Highway Administration. Office of Infrastructure Research and Development.

[40] Elshaer, M. (2017). Assessing the mechanical response of pavements during and after flooding. University of New Hampshire, Durham, 178. https://scholars.unh.edu/dissertation/160/

[41] Austroads (2019). Guide to Pavement Technology Part 2: Pavement Structural Design. Retrieved from: https://austroads.com.au/publications/pavement/agpt02

[42] Hicks, R. G., and Monismith, C. L. (1971). Factors Influencing the Resilient Response of Granular Materials. Highway Research Record 345, Washington, DC, pp. 15-31.

[43] Witczak, M. W., and Uzan, J. (1988). The Universal Airport Pavement Design System: Granular Material Characterization, University of Maryland, Department of Civil Engineering, MD

[44] ARA. (2004). Guide for Mechanistic-Empirical Pavement Design of New and Rehabilitated Pavement Structures. Final Report. NCHRP 1-37A. Washington, DC: National Cooperative Highway Research Program, Transportation Research Board.

[45] Al-Qadi, I. L., Wang, H., & Tutumluer, E. (2010). Dynamic Analysis of Thin Asphalt Pavements by Using Cross-Anisotropic Stress-Dependent Properties for Granular Layer. Transportation Research Record, 2154(1), 156–163. https://doi.org/10.3141/2154-16

[46] Gu, F., Luo, X., Luo, R., Lytton, R. L., Hajj, E. Y., & Siddharthan, R. V. (2016). Numerical modeling of geogrid-reinforced flexible pavement and corresponding validation using large-scale tank test. Construction and Building Materials, 122, 214–230. https://doi.org/10.1016/j.conbuildmat.2016.06.081

[47] Kim, M., Tutumluer, E., & Kwon, J. (2009). Nonlinear pavement foundation modeling for three-dimensional finite-element analysis of flexible pavements. International Journal of Geomechanics, 9(5), 195-208.

[48] Ali, H., Nowak, A. S., Michael Stallings, J., Chmielewski, J., Stawska, S., Ramesh Babu, A., & Haddadi, F. (2020). Impact of Heavy Trucks and Permitted Overweight Loads on Highways and Bridges Now and in the Future versus Permit Fees, Truck Registration Fees, and Fuel Taxes. Florida Department of Transportation. Research Center. Retrieved from: https://rosap.ntl.bts.gov/view/dot/56301

[49] Florida Traffic Online (2020). Florida Department of Transportation's Florida Traffic Online Web Application. Retrieved from: https://tdaappsprod.dot.state.fl.us/fto/

[50] The Modern-Era Retrospective analysis for Research and Applications (MERRA) Climate Data for MEPDG Inputs (2021). Retrieved from: https://infopave.fhwa.dot.gov/Tools/MEPDGInputsFromMERRA

[51] Qiao, Y., Flintsch, G. W., Dawson, A. R., & Parry, T. (2013). Examining effects of climatic factors on flexible pavement performance and service life. Transportation research record, 2349(1), 100-107.

[52] Kargah-Ostadi, N., Menendez, J. R., & Zhou, Y. (2018). Using Multi-Objective Optimization to Enhance Calibration of Performance Models in the Mechanistic-Empirical Pavement Design Guide (No. FHWA-HRT-17-104). The United States. Federal Highway Administration. Office of Research, Development, and Technology

[53] Duncan, J. M., Monismith, C. L., and Wilson, E. L. (1968). Finite Element Analyses of Pavements. Highway Research Record 228, TRB, National Research Council, Washington, DC, pp. 18-33.

[54] Tutumluer, E. (1995). Predicting Behavior of Flexible Pavements with Granular Bases, Ph.D. Dissertation, Georgia Institute of Technology, GA

[55] Pavement Interactive (2021). Reference Desk. Retrieved from https://pavementinteractive.org/reference-desk/

[56] Mallick, R. B., & El-Korchi, T. (2008). Pavement engineering. CRC Press, NY.

APPENDICES

APPENDIX A

GLOSSARY OF TERMS

Terms	Definition
Flexible Pavement	Pavement structures that are surfaced with asphalt material. These pavements are called flexible since the total pavement structure deflects due to traffic (wheel) loads, unlike concrete (rigid) pavements (55).
Asphalt Layer	The surface layer is in contact with traffic loads. It provides characteristics stated as friction, smoothness, noise control, rut resistance, and drainage. (55).
Base Layer	The layer is right below the asphalt layer. The base layer is known to "provide additional load distribution and contributes to drainage" (55). Base layers are usually constructed out of limerock in Florida.
Subbase Layer	The subbase layer is located between the base and subgrade layers. Its primary function is providing structural support, but this layer also lessens the intrusion of fines between subgrade and base layers (55).
Subgrade Layer	The natural (in-situ) materials or embankment upon which the pavement structure is constructed (56).
Resilient Modulus	Resilient modulus (M_R) is a measurement of the pavement materials' stiffness. The resilient modulus test follows the AASHTO T307 protocol to determine the elastic modulus based on the recoverable strain under repeated loads. It is defined as "the ratio of the amplitude of the repeated axial stress to the amplitude of the resultant recoverable axial strain" and typically determined in the units of psi (56).
Pavement Design Life	Design life is defined as "the time from original construction to a terminal condition for a pavement structure" (55). A terminal condition occurs when the pavement structure faces excessive distresses and needs reconstruction. Pavements are typically constructed for a specific design life (15 to 25 years).
Pavement Longevity	Pavement longevity is the actual service life of the flexible pavement.

Linear Elastic Pavement Analysis	Pavement analysis in which pavement layers are simplified as homogeneous, isotropic, linear elastic materials (38). Single resilient modulus values are assigned for each layer during the design life of the pavement structure.
Stress-dependent Nonlinear Pavement Analysis	Pavement analysis in which stress-dependent behavior of soils is considered during the design life of pavement structure. Soils can show either stress-hardening or stress-softening behavior. The resilient modulus of such soils can be estimated by using stress-dependent resilient modulus models (45). By applying the nonlinear material model, the variances created in horizontal and vertical directions of each layer can be considered for the structural pavement analysis.
User Material (UMAT) Subroutine	An interface offered by ABAQUS software to implement any specific material model which is not readily available within the software (38).

APPENDIX B

ENHANCED INTEGRATED CLIMATIC MODEL (EICM) SOIL WATER CHARACTERISTIC CURVE (SWCC) MODEL AND FITTING PARAMETERS

Soil moisture within the EICM model is considered by soil water characteristic curves (SWCCs), which describe the relationship between the soil matric suction and the degree of saturation of soil (S). The SWCC relationship model was proposed by Fredlund and Xing (36) to calculate the degree of saturation from matric suction as presented in Equation B.1 and Equation B.2.

$$S = C(h) \times \left[\frac{1}{\left[\ln\left[\exp(1) + \left(\frac{h}{a_f} \right)^{b_f} \right] \right]^{c_f}} \right] \qquad \text{Equation B. 1}$$

$$C(h) = \left[1 - \frac{\ln\left(1 + \frac{h}{h_r} \right)}{\ln\left(1 + \frac{10^6}{h_r} \right)} \right] \qquad \text{Equation B. 2}$$

where:

S = degree of saturation

h = matric suction

a_f, b_f, c_f, h_r = fitting parameters to the equation

Witzcak et al. (37) developed a methodology to determine the fitting parameters for various soil types based on their properties as shown below:

- **For non-plastic soils (Plasticity Index = 0),**

$a_f = 1.14 \times a - 0.5$
$a = -2.79 - 14.1 \times \log(D_{20}) - 1.9 \times 10^{-6} \times P_{200}{}^{4.34} + 7 \times \log(D_{30}) + 0.55 \times D_{100}$
$D_{100} = 10^{\left[\frac{40}{m_1} + \log(D_{60})\right]}$
$m_1 = \frac{30}{\left[\log(D_{90}) - \log(D_{60})\right]}$
$b_f = 0.936 \times b - 3.8$
$b = \left\{5.39 - 0.29 \times \ln\left[P_{200}\left(\frac{D_{90}}{D_{10}}\right)\right] + 3 \times D_0{}^{0.57} + 0.021 \times P_{200}{}^{1.19}\right\} \times m_1{}^{0.1}$
$D_0 = 10^{\left[\frac{-30}{m_2} + \log(D_{30})\right]}$
$m_2 = \frac{20}{\left[\log(D_{30}) - \log(D_{10})\right]}$
$c_f = 0.26 \times e^{0.758 \times c} + 1.4 \times D_{10}$
$c = \log(m_2{}^{1.15}) - \left(1 - \frac{1}{b_f}\right)$
$h_r = 100$

These equations have the following constraints:

If $a_f < 1$, then $a_f = 2.25 \times P_{200}{}^{0.5} + 5$

$3 < b_f < 4$

a_f, b_f, c_f, h_r = SWCC fitting parameters

D_{10} = Grain diameter corresponding to 10% of passing by weight, in mm

D_{20} = Grain diameter corresponding to 20% of passing by weight, in mm

D_{30} = Grain diameter corresponding to 30% of passing by weight, in mm

D_{60} = Grain diameter corresponding to 60% of passing by weight, in mm

D_{90} = Grain diameter corresponding to 90% of passing by weight, in mm

P_{200} = Percent passing US standard sieve #200

- **For plastic soils (Plasticity Index > 0):**

$a_f = 32.835 \times \{\ln(wPI)\} + 32.438$
$b_f = 1.421 \times (wPI)^{-0.3185}$
$c_f = -0.2154 \times \{\ln(wPI)\} + 0.7145$
$h_r = 500$

The constraints required for these equations are:

If $a_f < 5$, then $a_f = 5$, If $c_f < 5$, then $c_f = 0.03$

where: $wPI = P_{200} \times$ Plasticity Index (PI)

APPENDIX C

ABAQUS FINITE ELEMENT MODEL DOMAIN SIZE DETERMINATION

Figure C.1 shows the control pavement structure used for KENLAYER linear pavement analysis. Four structural layers selected were asphalt concrete, LBR100 limerock base, LBR40 subbase, and the subgrade soil. A tire with 80 psi contact pressure with a 6 inches contact radius was selected as representative wheel load. Several linear elastic finite-element analyses with different domain sizes were conducted to determine the most representative domain size. Linear finite-element model analysis results, then, were compared with the KENLAYER software's linear analysis results.

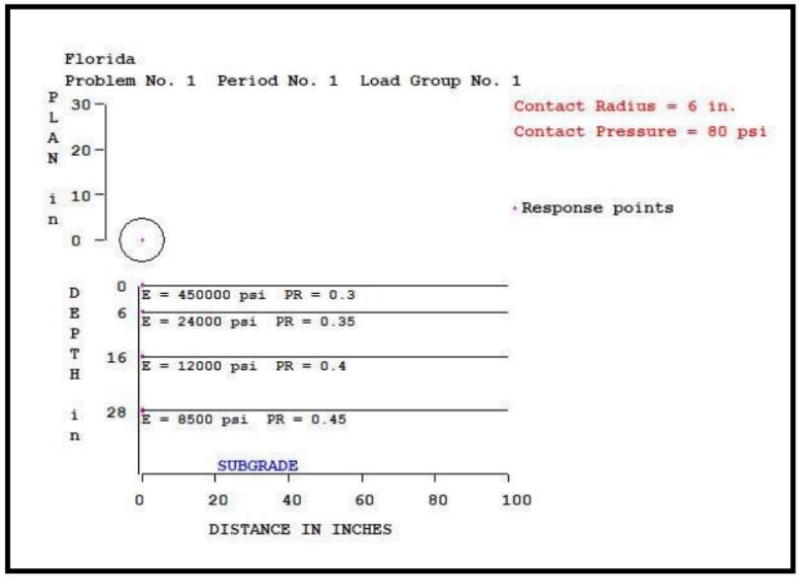

Figure C. 1 The selected control pavement structure and material properties used for KENLAYER linear analysis

Figure C.2 compares analysis results from KENLAYER software and ABAQUS software with the different domain sizes. The domain size of 20-times the radius of the loading area in the horizontal direction and 125-times the radius of the loading area in the vertical order (20 x 125) showed the closest results to the linear analysis solutions.

		Finite Element Analysis Domain Size					
Pavement Response	KENLAYER	12 X 50	20 x 100	20 X 120	20 X 125	20 x 140	25 X 140
Surface Deflection (inches)	0.0213	0.0186	0.0203	0.0210	0.0212	0.0218	0.0209
Horizontal strain at bottom of AC (microstrain)	235	230	230	231	231	231	231
Vertical stress on top of Subgrade (psi)	2.4	2.5	2.4	2.5	2.5	2.5	2.5
Vertical strain on top of Subgrade (microstrain)	260	247	269	260	260	260	262

Figure C. 2 ABAQUS finite element analysis results for the domain size determination efforts

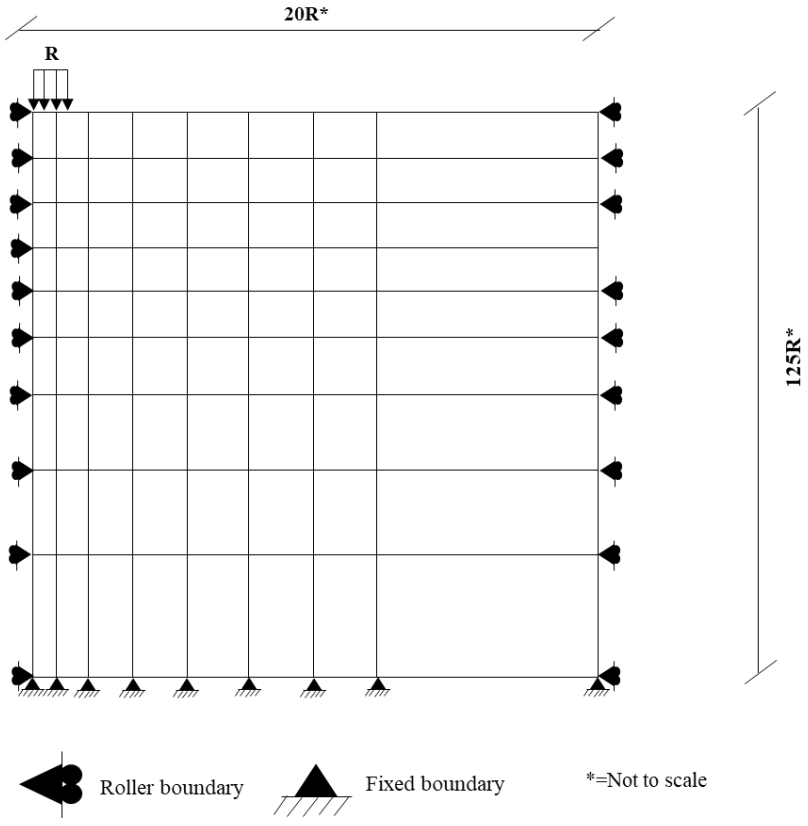

Figure C. 3 The selected ABAQUS domain size for the nonlinear analysis

VITA

MEHMET GOKSEL GOCMEZ

Born, Mersin, Turkey

2011-2016	B.S., Civil Engineering Yildiz Technical University Istanbul, Turkey

PUBLICATIONS AND PRESENTATIONS

Rojali, A., Gocmez, M. G., Ali, H. A., & Fuentes, H. R. (2021). Improvement and Benefit of Updated Vulnerability Maps of Pavement Infrastructure Affected by Sea-Level Rise: A Case in South Florida. Asia Oceanic Geosciences Society: 18th Annual Meeting